Since January 2020 Elsevier has created a COVID-19 resource centre with free information in English and Mandarin on the novel coronavirus COVID-19. The COVID-19 resource centre is hosted on Elsevier Connect, the company's public news and information website.

Cell

A defective viral genome strategy elicits broad protective immunity against respiratory viruses

Graphical Abstract

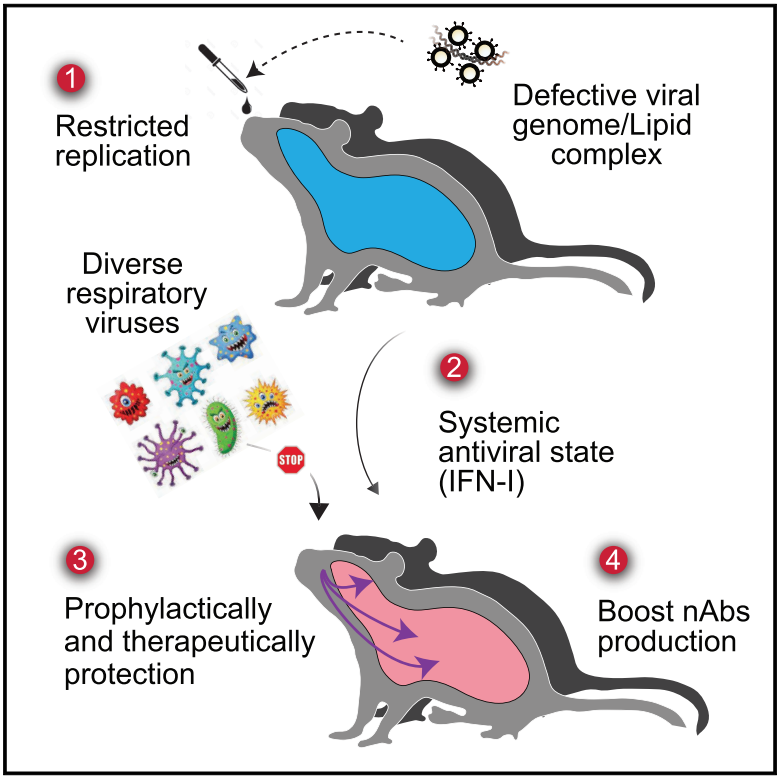

Highlights

- eTIP1 is a novel tool to protect against viral infections, including SARS-CoV-2 strains
- Intranasal eTIP1 delivery elicits innate antiviral responses in the respiratory tract
- eTIP1 provides pre- and post-exposure protection against respiratory viral infections
- eTIP1 treatment boosts generation of protective antibodies against pathogenic virus

Authors

Yinghong Xiao, Peter V. Lidsky, Yuta Shirogane, ..., Peter K. Jackson, Judith Frydman, Raul Andino

Correspondence

raul.andino@ucsf.edu

In brief

A defective viral genome derived from poliovirus induces type I interferon-mediated prophylactic and therapeutic effects against respiratory viruses, including SARS-CoV-2 and influenza, in mouse infection models.

Xiao et al., 2021, Cell *184*, 6037–6051
December 9, 2021
https://doi.org/10.1016/j.cell.2021.11.023

CellPress

Cell

CellPress

Article

A defective viral genome strategy elicits broad protective immunity against respiratory viruses

Yinghong Xiao,[1] Peter V. Lidsky,[1] Yuta Shirogane,[1,2] Ranen Aviner,[1,3] Chien-Ting Wu,[4] Weiyi Li,[1] Weihao Zheng,[5] Dale Talbot,[1,6] Adam Catching,[1] Gilad Doitsh,[1] Weiheng Su,[1,7] Colby E. Gekko,[1] Arabinda Nayak,[1,3] Joel D. Ernst,[5] Leonid Brodsky,[8] Elia Brodsky,[9] Elsa Rousseau,[10] Sara Capponi,[10] Simone Bianco,[10] Robert Nakamura,[6] Peter K. Jackson,[4] Judith Frydman,[3] and Raul Andino[1,11,*]

[1]Department of Microbiology and Immunology, University of California, San Francisco, San Francisco, CA 94158, USA
[2]Department of Virology, Faculty of Medicine, Kyushu University, Fukuoka, Japan
[3]Department of Biology and Genetics, Stanford University, Stanford, CA 94305, USA
[4]Baxter Laboratory for Stem Cell Biology, Department of Microbiology & Immunology, Stanford University, Stanford, CA 94305, USA
[5]Division of Experimental Medicine, Department of Medicine, University of California, San Francisco, San Francisco, CA 94110, USA
[6]Aleph Therapeutics, Inc., Stanford, CA 94305, USA
[7]School of Life Sciences, Jilin University, Changchun, China
[8]Tauber Bioinformatics Research Center and Department of Evolutionary & Environmental Biology, University of Haifa, Mount Carmel, Haifa 31905, Israel
[9]Pine Biotech Inc., New Orleans, LA 70112, USA
[10]Functional Genomics and Cellular Engineering, AI and Cognitive Software, IBM Almaden Research Center, San Jose, CA 95120, USA
[11]Lead contact
*Correspondence: raul.andino@ucsf.edu
https://doi.org/10.1016/j.cell.2021.11.023

SUMMARY

RNA viruses generate defective viral genomes (DVGs) that can interfere with replication of the parental wild-type virus. To examine their therapeutic potential, we created a DVG by deleting the capsid-coding region of poliovirus. Strikingly, intraperitoneal or intranasal administration of this genome, which we termed eTIP1, elicits an antiviral response, inhibits replication, and protects mice from several RNA viruses, including enteroviruses, influenza, and SARS-CoV-2. While eTIP1 replication following intranasal administration is limited to the nasal cavity, its antiviral action extends non-cell-autonomously to the lungs. eTIP1 broad-spectrum antiviral effects are mediated by both local and distal type I interferon responses. Importantly, while a single eTIP1 dose protects animals from SARS-CoV-2 infection, it also stimulates production of SARS-CoV-2 neutralizing antibodies that afford long-lasting protection from SARS-CoV-2 reinfection. Thus, eTIP1 is a safe and effective broad-spectrum antiviral generating short- and long-term protection against SARS-CoV-2 and other respiratory infections in animal models.

INTRODUCTION

RNA viruses pose a continuing worldwide health threat. Each new epidemic, from HIV to influenza to dengue and Zika to SARS-CoV-2, highlights an urgent need for effective antiviral drugs and interventions (Meganck and Baric, 2021). The highly contagious coronavirus disease 2019 (COVID-19) (Zhu et al., 2020) has caused more than 200 million cases and nearly 5 million deaths, and the numbers are still increasing (WHO, 2021). Despite development of severe acute respiratory syndrome coronavirus 2 (SARS-CoV-2) vaccines, the virus is still circulating (Cohen et al., 2021; Deng et al., 2021; Guo et al., 2021; Kang et al., 2021; Abdool Karim and de Oliveira, 2021; Rappazzo et al., 2021; Sun et al., 2021; Zhou et al., 2021). A few antivirals and monoclonal antibodies are available for SARS-CoV-2 therapy (Canedo-Marroquín et al., 2020; Gonçalves et al., 2021; Lundstrom, 2020), but the high mutation rate of the RNA virus is likely to give rise to resistant variants. Clearly, novel therapeutics with a low risk of drug resistance are essential to combat COVID-19 and future epidemics. Unfortunately, developing broad-spectrum antiviral strategies is extremely challenging (Geller et al., 2012; Meganck and Baric, 2021; Tse et al., 2020).

One attractive strategy would be to harness the effective antiviral defenses of the host. Viral infections elicit a range of responses that prevent or attenuate most infections. Indeed, even for viruses such as influenza virus or SARS-CoV-2, most infections are asymptomatic (Cohen et al., 2021; Lutrick et al., 2021; Zhang et al., 2021). However, harnessing these responses is difficult. First, most viruses have mechanisms to inactivate or dampen innate immunity, often at multiple steps of the pathway (Kikkert, 2020). Second, direct interventions to induce these responses, such as intravenous administration of interferon, have undesirable side effects, likely because they override the delicate regulatory balance that keeps beneficial innate immunity from damaging tissues (Guo et al., 2021; Nelemans and Kikkert, 2019).

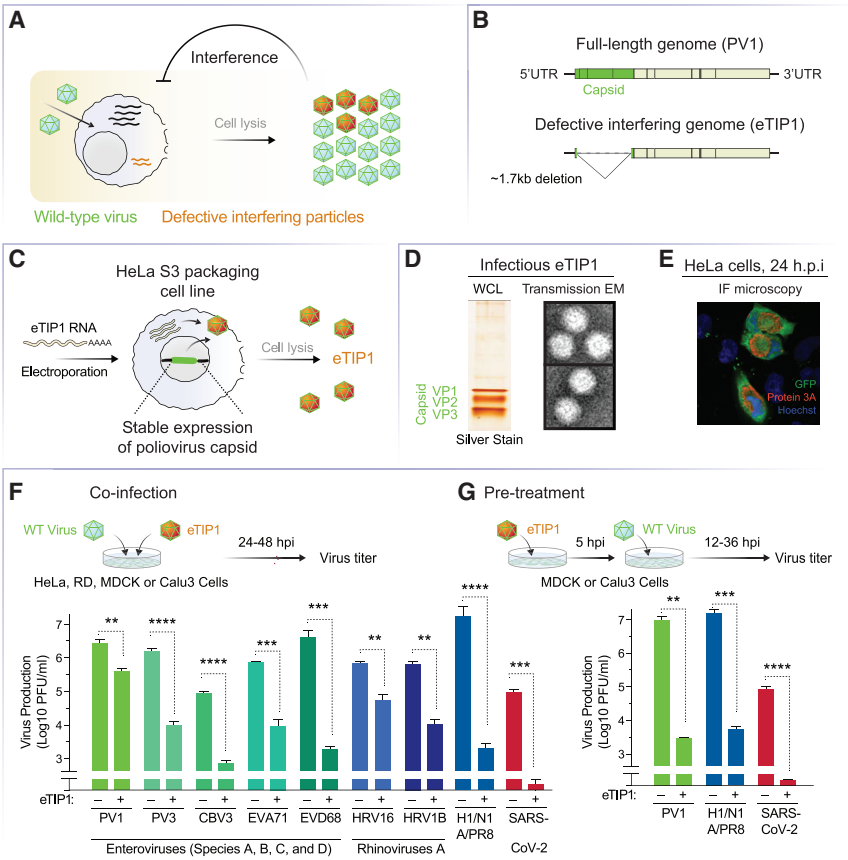

Figure 1. An engineered defective interfering particle derived from PV confers broad-spectrum antiviral protection in cell-culture models

(A) During replication, RNA virus produces defective viral genomes (DVGs) that attenuate parental virus replication and pathogenesis.

(B) Schematic representation of the WT PV1 and the engineered DVG genome, herein called eTIP1. The structural genes (capsid, green) encode viral capsid proteins, and the non-structural coding region (yellow) encodes the enzymatic machinery required for replication. eTIP1 carries a large deletion of ~1,700 bases in the capsid proteins of PV1 virus, and GFP-Venus gene was inserted at the N terminus of the engineered viral polyprotein.

(C) Production of eTIP1 particles. *In-vitro* transcribed RNA was transfected into a packaging cell line that expresses the precursor for poliovirus capsid proteins (HelaS3/P1). eTIP1s were passaged three times in HeLaS3/P1 cells to generate higher titer eTIP1 stocks (~10^7 infectious units/mL).

(D) eTIP1 were purified by sucrose gradient and examined by SDS-polyacrylamide gel electrophoresis with silver staining and electron microscopy and negative staining.

(E) eTIP1 replication in cell culture. HeLa cells were infected with eTIP1 at an moi = 1, and 24 h post-infection, HelaS3 cells were fixed and analyzed by immunostaining with antibodies to polio-3A antibody (red) and GFP (green), and DAPI (blue).

(F) eTIP1 inhibits a wide range of enterovirus subspecies in cell culture (e.g., PV1 and 3, coxsackievirus B3 (CVB3), enterovirus A71 (EV-A71), enterovirus D68 (EV-D86), rhinovirus 16 (HRV16), rhinovirus 1A (HRV1A), influenza virus A virus (H1/N1, A/PR8), and SARS-CoV-2.

(G) eTIP1 inhibits replication PV1, A/PR8, SARS-CoV-2. Cells were pretreated with eTIP1 with moi = 5 for 5 h, and then cells were infected with PV1, H1/N1 A/PR8, SARS-CoV-2 at moi = 0.1. Significance was calculated using a two-tailed Student's t test. **p < 0.01; ***p < 0.001; and ****p < 0.0001.

The innate immune system evolved tightly regulated mechanisms to protect from viral infection and prevent damage to the host. The challenge is to harness these beneficial responses without triggering detrimental side-effects. Our strategy was based on an unexpected and remarkable observation from early epidemiological studies of the Sabin poliovirus (PV) vaccine. Immunization with attenuated Sabin PV protected from PV infection and also reduced influenza virus morbidity by almost fourfold. It even accelerated healing of genital lesions caused by herpes simplex virus. These benefits were never observed upon immunization with an inactivated PV virus (e.g., Salk vaccine). Importantly, the Sabin vaccine causes none of the severe side-effects of interferon administration (Chumakov et al., 2020, 1991). These puzzling observations raise the hypothesis that a non-pathogenic virus or virus-like entity could safely stimulate the host innate antiviral responses.

To test this hypothesis, we developed an engineered virus-like entity, based on a defective viral genome (DVG), and tested its potency as a broad-spectrum antiviral. Due to the high error rate of their RNA-dependent RNA-polymerases, RNA viruses naturally generate genome deletions with various degrees of viability (Crotty and Andino, 2002; Crotty et al., 2001; Domingo et al., 1996, 2002; Peersen, 2017; Pfeiffer and Kirkegaard, 2003). These DVGs are maintained by co-infection with the parental virus (Dimmock and Easton, 2014, 2015; Easton et al., 2011; Goff et al., 2012; Huang and Baltimore, 1970; Kim et al., 1998; Kitamura et al., 1981; McClure et al., 1980; Perrault, 1981; Perrault and Semler, 1979; Shirogane et al., 2019; Vignuzzi and López, 2019), but lack critical portions of the viral genome and therefore cannot propagate or cause disease on their own. DVGs attenuate replication of their corresponding parental virus in a process known as viral interference, first described in the 1960s (Huang and Baltimore, 1970; McClure et al., 1980; Vignuzzi and López, 2019) (Figure 1A). These findings led to speculation that DVGs modulate the course of disease, perhaps by outcompeting the full-length virus for cellular resources (Rezelj et al., 2021; Vignuzzi and López, 2019). However, the mechanism and therapeutic potential of viral interference are poorly understood.

We engineered a PV-derived DVG that can be delivered by lipid nanoparticles and is highly effective at preventing replication of respiratory viruses, including rhinovirus, influenza virus and SARS-CoV-2 in cell and animal models. The DVG blocks viral replication by inducing an antiviral state in the respiratory tract. It can be administered intranasally, as pre- or post-exposure prophylaxis, to protect mice from pathogenic viruses without detrimental side-effects. Indeed, eTIP1 (enteroviral therapeutic interfering particle 1) infectious particles protect even

when administered 24–48 h post-infection with SARS-CoV-2, PV, coxsackievirus B3 (CBV3), and influenza virus. Importantly, eTIP1 reduces virus load by several orders of magnitude and also enables generation of neutralizing antibodies against the challenging virus. This enhanced antibody response provides long-term protection from reinfection, lasting weeks after the initial intervention. We suggest that our approach is an effective, non-invasive, broad-spectrum strategy to block viral infections, including SARS-CoV-2.

RESULTS

Engineering a defective poliovirus genome as a broad-spectrum antiviral

We engineered a DVG for PV type 1 (PV1) by replacing the entire P1 region, which encodes structural proteins, with GFP (Figure 1B). eTIP1 infectious particles were produced using a packaging HeLa cell line that stably expresses the PV1 capsid protein precursor P1 (HelaS3/P1) (Figure 1C). Transfection of HeLaS3/P1 with *in vitro* transcribed eTIP1 RNA generated eTIP1 infectious particles that were amplified by repeated infection of HelaS3/P1. High-titer (>10^8 infectious units [IUs]/mL) were purified by sucrose cushion and gradients to 95% purity, as determined by silver stain-polyacrylamide gel electrophoresis and negative-staining electron microscopy (EM) (Figure 1D). eTIP1s were similar in size to wild-type (WT) PV1 particles (PV1 radius = 27.07 ± 1.02 nm and eTIP1 radius = 27.51 ± 1.01 nm). Purified eTIP1 particles can infect cells, as determined by expression of GFP and immunofluorescence (I.F.) with polio-3A antibody (Figures 1E and S1A). Importantly, eTIP1s cannot spread from cell to cell without a WT PV1 acting as a helper virus (Dimmock and Easton, 2015; Perrault and Semler, 1979; Shirogane et al., 2021a; Vignuzzi and López, 2019).

To test the therapeutic potential of eTIP1s, we tested if it could block replication of PV1 and related enteroviruses of clinical importance. To this end, we infected cells with enteroviruses with and without eTIP1s at a ratio of 1:20 (eTIP1 multiplicity of infection [moi] = 1–5). eTIP1s effectively blocked replication of PV1 and other enteroviruses, including enterovirus EV-D68, EV-A71, CVB3, and rhinoviruses (Figures 1F and S1B). Virus replication was inhibited 10- to 1,000-fold, depending on the virus and cell line (Figure 1F). To determine if eTIP1 antiviral activity is restricted to the genus of its parental virus, we next examined its activity against an unrelated virus. eTIP1 co-infection at a ratio of 1:50 inhibited influenza A (A/PR8) and SARS-CoV-2 by 100- to 1,000-fold (Figure 1F). Antiviral activity was even stronger when eTIP1 was administered 5 h before infection with PV1, A/PR8, or SARS-CoV-2 (Figure 1G). These results suggest that the inhibitory activity of eTIP1 does not rely on direct competition for enteroviral proteins, such as the viral capsid or other viral or host factors required for enterovirus replication.

eTIP1 prevents lethal infection in mice

Given the broad-spectrum inhibitory effects of eTIP1s in cell culture, we examined their ability to prevent disease in mice infected with several pathogenic viruses. After intraperitoneal (IP) inoculation of susceptible mice, PV1 replicates and accumulates to high titers in diverse tissues, ultimately reaching the central nervous system (CNS) to cause paralysis and death (Ida-Hosonuma et al., 2005; Ohka et al., 2007; Pfeiffer, 2010; Xiao et al., 2017). Similarly, after intranasal (IN) inoculation, PV1 reaches the CNS rapidly through the olfactory nerve, causing severe disease (Nagata et al., 2004).

We infected mice by the IP route with high doses of PV1 (10^7 plaque-forming units, pfu) with or without co-inoculation with eTIP1s (Figure 2A, *i*, IP). Under these conditions, eTIP1 significantly attenuated disease and protected 80%–90% of mice from lethal infection. Importantly, co-inoculation of eTIP1s inactivated by UV irradiation did not protect mice from PV1, indicating that the eTIP1s must be replication competent to exert its antiviral properties. This experiment ruled out that protection was conferred by a contaminant introduced in eTIP1 production. eTIP1s also protected animals from disease (weight loss) and death after infection with a non-polio enterovirus, CVB3 (Figures S2A and S2B). Next, we determined if eTIP1 protects animals from respiratory infection. IN co-inoculation of PV1 and eTIP1s protected from death (Figure 2A, *ii*) and reduced PV1 viral loads in spleen and brain over 500-fold (Figure S1C).

To determine if eTIP1-induced protection is long lasting, we administered a single IN dose of eTIP1 and challenged the mice with pathogenic PV1 48 h later. While animals inoculated with PV1 alone succumbed to infection, pre-exposure administration of eTIP1 protected 90% of the animals from lethal disease (Figure 2B, *i*). Post-exposure administration of eTIP1 24 and 48 h after PV1 infection also elicited significant protection (Figure 2B, *ii*). The protective effects were lost if treatment is initiated 72 h after PV1 infection (not shown). These results indicate that both pre- and post-exposure prophylaxis with eTIP1 protects against IN PV1 infection, preventing severe disease and death. In addition, eTIP1 protected from infection with A/PR8 and CVB3 when administered 24 (A/PR8 and CVB3) (Figure 2C, *ii*, and Figure S1D) or 48 h (CVB3) after the viral challenge (Figure 2C, *i*). This indicates that eTIP1 can protect from respiratory infections after a single IN dose.

Intranasal inoculation of eTIP1 lipid nanoparticles and its replication tissue distribution

Our finding that eTIP1s interfere with viral infection in mice supports their use as an antiviral. However, their applicability may be limited by practical considerations such as a requirement for the PV receptor (PVR) to enter target cells and neutralization in vaccinated individuals. We thus tested whether eTIP1 DVG could be delivered by synthetic nanostructured lipid/RNA complexes (herein lipid nanoparticles, or LNPs). LNPs deliver RNA via endocytosis, which is unaffected by pre-existing immunity, and so may be administered as multiple consecutive doses (Figure 3A). We chose a cationic lipid formulation that binds well to the phosphate backbone of nucleic acids, and is easy to prepare, non-toxic, and extensively characterized (Kranz et al., 2016; Scheideler et al., 2020). We find that LNPs protect RNA molecules from hydrolysis and enable eTIP1 delivery to initiate replication at mucosal reparatory surfaces. We confirmed that LNPs deliver synthetic eTIP1 RNA in cell cultures (Figure S3A). Then, we compared the site of eTIP1 replication when delivered to mice via IN administration of particles or LNPs. At 24 h post-inoculation, immunohistochemistry of mouse heads and lungs

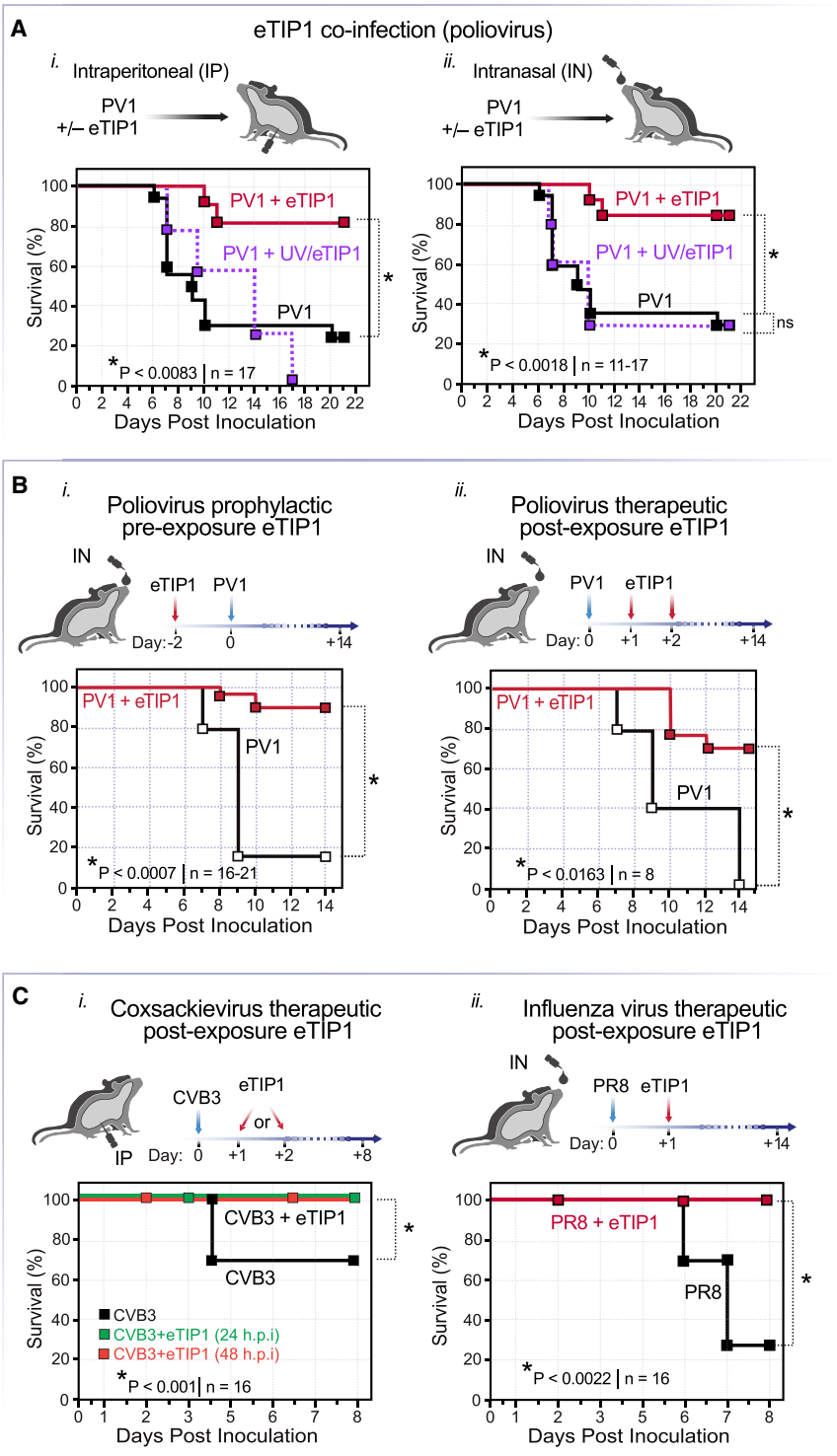

Figure 2. eTIP1 protects against poliovirus (PV1), coxsackievirus B3 (CVB3), and influenza virus (H1/N1, A/PR8) in mouse models of infection

(A) (i) IP inoculation in immune-competent C57BL6 TgPVR mice with 10^7 pfu poliovirus (PV1) or co-infected eTIP1 at a ratio of 1:10. As a control, PV1 was co- inoculated with UV-inactivated eTIP1 (UV/eTIP1). Black line represents PV1 alone. Red line represents co-infected mixed PV1+ eTIP1 group. Purple line represents co-infected mixed PV1 with UV/eTIP1. (ii) IN inoculation. C57BL6 TgPVR mice were infected with 3×10^5 pfu PV1 IN or co-infected eTIP1 or UV/eTIP1, at ratio 1:20. Color code as in (i). *p < 0.001.

(B) Pre-exposure and post-exposure prophylaxis. (i) eTIP1 (6×10^6 IU) was inoculated into C57BL6 TgPVR mice intranasally, and 48 h later mice were challenged with 3×10^5 pfu of pathogenic PV1. (ii) C57BL6 mice were infected with 3×10^5 pfu PV1 C57BL6, and 1 and 2 days post-infection animals were treated IN with 6×10^6 IU eTIP1. n = 16–21.

(C) (i) Post-exposure effects of eTIP1 treatment on coxsackievirus. C57BL6 mice were infected with 10^5 pfu CVB3 by the IP route (black line), and at 24 (green line) or 48 h (red line), animals were IP inoculated with 10^7 IU eTIP1 (n = 7–9). (ii) Therapeutic effects of eTIP1 on influenza virus. C57BL6 mice were infected with 10^5 pfu influenza A/PR8 IN, and then 6×10^6 IU eTIP1 were inoculated IN at 24 h post-infection (n = 16). In (A), (B), (F), and (E), the statistical analysis of survival curves was performed by log-rank (Mantel-Cox) test. Significance is noted with asterisks; ns, not significant.

detected eTIP1 replication in epithelial cells within the ethmoid turbinates of the upper respiratory nasal cavity (Figure 3B). eTIP1 replication was limited to those tissues, not detected in other regions of the respiratory tract, and observed for only 12–24 h post-inoculation.

We next tested if eTIP1 can be mobilized from the site of inoculation to other tissues by a co-infecting help virus. We co-inoculated highly susceptible mice ($IFNAR^{-/-}$) intramuscularly with 200 pfu of PV1 with eTIP1s (50,000 IUs). The high concentration of the initial inoculum at the site of injection increases the probability PV1 and eTIP1 co-infection, enabling trans-encapsidation of eTIP1s by PV1 structural proteins. Using $IFNAR^{-/-}$ mice increases susceptibility to PV infection and the rapid spread of the virus to diverse tissues. We examined PV1 and eTIP1 replication in muscle, spleen, and spinal cord by RT-qPCR. eTIP1 RNA accumulated at the site of inoculation on days 1 and 3 and decayed by day 6 (Figure S3B). eTIP1 RNA was barely or not detected in spleen or spinal cord, indicating that the eTIP1 does not spread beyond the site of inoculation even with PV1 (Figure S3B). $IFNAR^{-/-}$ mice inoculated only with eTIP1s showed no sign of distress and survived inoculation for several weeks (Figure S3C). Thus, eTIP1 replication is restricted to the site of initial replication (i.e., muscle [IM] or nasal turbinates [IN]).

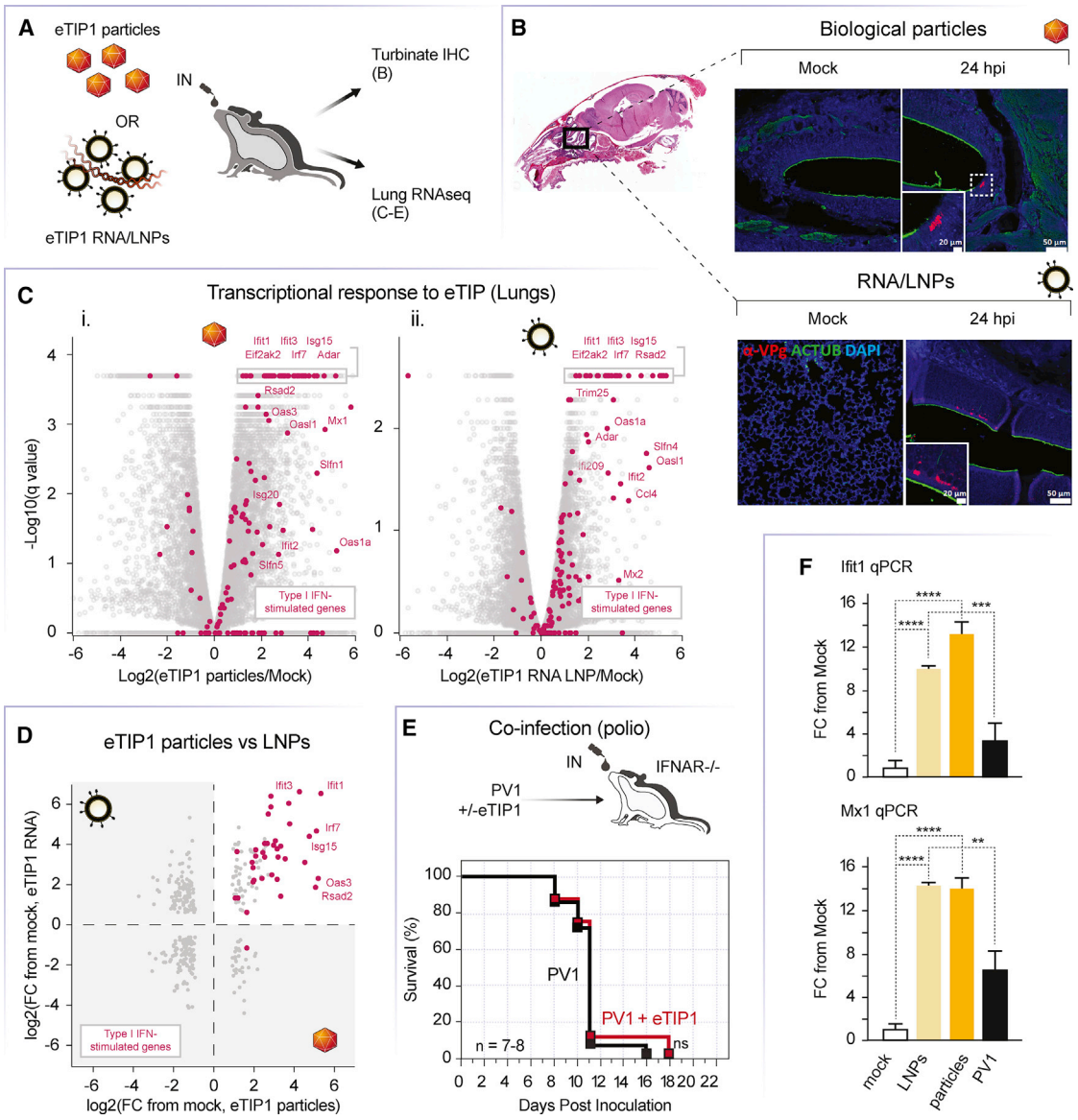

Figure 3. eTIP1 protects against PV through a type I IFN response

(A) Schematic representation of the eTIP1 biological particles and eTIP1 RNA complex with LNPs. Animals were analyzed 24 h after IN intranasal inoculation by immune histochemistry (IHC) or by RNA-seq transcriptome profiling of the lung gene expression.

(B) eTIP1 site of replication within the respiratory tract. Mice were inoculated IN with 30 μg of eTIP1 RNA or mock (PBS with empty LNPs) or infected with 6×10^6 infectious units of eTIP1. Heads of inoculated animals were analyzed 24 h post-inoculation by IHC. Heads and lungs were collected and fixed in 4% para-formaldehyde (PFA), embedded in paraffin wax, and cut into 5-μm sections. eTIP1s and eTIP1 RNA were stained using PV antibody VPg (3B protein). VPg (3B) (red), ACTUB (green), nuclear (blue). eTIP1 replication was restricted to the upper respiratory nasal cavity. We observed no replication in the lungs.

(C) C57BL6 TgPVR mice were infected with 6×10^6 IU eTIP1 particles or PBS (mock) (i), or animals were inoculated IN with 30 μg eTIP1 LNP or mock (empty LNP). Lung tissues were collected 24 (eTIP1 LNP) or 48 h (eTIP1 particles) post-inoculation, and mRNA was isolated from these tissues and examined by RNA-seq. Volcano plot shows pairwise comparisons of mRNA levels in infected versus mock-infected lung tissues and represented as a volcano plot of the genes with significant changes in expression, compared to the mock-treated group (false discovery rate, q-value < 0.05). n = 3 on two experimental replicates.

(D) Pairwise comparison of eTIP1 RNA/LNP versus eTIP1 particle in lung of infected animal. Red dots represent type I IFN genes.

(E) eTIP1 fails to protect against PV1 (IN in mice lacking IFNAR$^{-/-}$. IFNAR$^{-/-}$ mice were infected with 5×10^4 pfu PV1 alone or co-infected with mixed PV1 + eTIP1 at a ratio of 1:20 by IN route. Black line represents PV1 alone. Red dash line represents co-infected mixed PV1+ eTIP1 group (n = 7-10). Data were collected from two independent experiments. The comparison of survival curves was performed by log-rank (Mantel-Cox) test. ns, not significant.

(F) RT-qPCR validation of upregulated genes in lungs of animals treated with eTIP1. K18-hACE2 mice were transfected with 30 μg of eTIP1 RNA or infected with 6×10^6 IU of eTIP1 particles or PV1. As control, we mock-infected animals (PBS with empty LNPs, lipofectamine 2000) for 24 h. Lungs were collected, and total RNA was extracted with Trizol reagents. RT-qPCR were performed to qualify the IFN-induced genes MX1 and ISG56 (IFIT1), n = 3, normalized to GAPDH. Unpaired Student's t tests. *p < 0.05; **p < 0.01; ***p < 0.001.

Role of interferon in eTIP1-mediated antiviral protection

We next sought to determine the mechanism by which eTIP1 induces the antiviral protective effect. We considered two possible models. In one, DVGs, whose shorter genomes may provide a replication advantage, outcompete the full-length viral genome for cellular resources and encapsidation by structural proteins, thus impairing propagation of parental virus to other cells in the tissue (Shirogane et al., 2021b; Vignuzzi and López, 2019). In the second, DVGs induce an innate response that cross-protects from other viral infections. Self-replicating RNAs, particularly DVGs that form cytosolic double-stranded RNA (dsRNA) intermediates, activate pattern recognition receptors, and trigger innate immune responses that lead to production of interferon (IFN)-stimulated genes (ISGs) (Brennan and Bowie, 2010; Finlay and McFadden, 2006; Kikkert, 2020; Narayanan and Makino, 2009; Vignuzzi and López, 2019). In this way, DVGs may induce a systemic antiviral state that interferes with replication of WT virus. In addition, DVGs may cause cells to lose the integrity of their plasma membrane and release damage-associated molecules that recruit various types of circulating leukocytes to the site (Preissner et al., 2020). While the first option requires co-infection of DVG and WT virus for interference to occur, the second model is consistent with DVGs impairing WT virus replication in a non-cell-autonomous manner. Our data are consistent with the second mechanism.

To test this hypothesis, we performed unbiased transcriptome profiling in lungs of eTIP1- or mock (PBS)-treated mice (Figure 3A). Whole lungs were harvested at 1 or 2 days post-IN administration of either 6×10^6 IUs of eTIP1s or 30 μg of eTIP1 RNA in LNPs. RNA sequencing (RNA-seq) analysis showed that both methods induced a common set of bona fide type I IFN-responsive genes (Schoggins and Rice, 2011; Schoggins et al., 2011, 2014; Xiao et al., 2017), including Ifit1-3, Eif2ak2 (PKR), Irf7, Isg15, Rsad2, Mx1, Adar, and a number of Oas paralogs (Figures 3C). Type I ISGs were similarly induced regardless of delivery method (Figures 3D and S4B). This was confirmed by RT-qPCR analysis of two ISGs, Mx1 and Ifit, in lungs of mice inoculated with eTIP1s or LNPs (Figure 2F). These genes were also induced at 24 h post-infection with PV1, albeit to lower levels (Figure 2F). This suggests that the IFN response is stronger without the capsid coding region of PV1. Foot-and-mouth disease virus capsid protein VP3 inhibits IFN signaling (Li et al., 2016a, 2016b). Thus, IN delivery of eTIP1 as biological particles or LNPs stimulates a more robust innate immune response than WT PV.

These experiments suggest that eTIP1 induces an IFN-mediated antiviral state. Next, we directly tested whether eTIP1-mediated antiviral protection requires systemic innate immune stimulation of an IFN response. We tested the capacity of eTIP1 to protect animals lacking the IFN-α/β receptor ($IFNAR^{-/-}$) against PV1 infection. Under conditions in which eTIP1 elicits a robust protective activity in immunocompetent WT mice (Figure 2), the antiviral protection is completely lost in animals lacking the IFN-α/β receptor ($IFNAR^{-/-}$; Figures 3E and S4B). This indicates that IFN-I responses are important for the eTIP1-mediated protection from IP and IN infection with pathogenic PV1.

Pre- and post-exposure eTIP1 treatment protects from SARS-CoV-2

Next, we determined if eTIP1 protects animals from SARS-CoV-2 infection. At 24 h after a single IN dose of eTIP1 LNPs, we infected K18-hACE2 mice with 6×10^4 pfu SARS-CoV-2 (D614G variant). We measured the effects of eTIP1 on SARS-CoV-2 replication in clinically relevant tissues (i.e., lungs and brains) collected on days 3 and 6 post-infection. SARS-CoV-2 replication was detected by plaque assay and RT-qPCR, as well as immunohistochemistry with antibodies against the nucleocapsid proteins (NPs) and spike proteins (SPs). As expected, mice pretreated with control LNPs had significant SARS-CoV-2 titers and widespread NP and SP immunoreactivity throughout the lung and brain (Figures 4A–4C). Pretreatment with eTIP1 LNPs lowered SARS-CoV-2 titers and viral RNA copies by 2–3 logs (Figure 4A) and reduced immunoreactivity in lungs and brains (Figures 4B and 4C). Inoculation of LNPs carrying eTIP1 inactivated by UV, a replication-incompetent eTIP1 RNA carrying a large deletion of the 3′ of the genome (truncated PvuII), or poly IC did not protect mice from SARS-CoV-2 infection (Figure S5A), indicating that eTIP1s must be replication competent to protect from SARS-CoV-2 infection, as shown earlier (Figure 2A).

We also tested if eTIP1s protect against other variants of concern or interest (VOCs or VOIs), including B.1.1.7 (Alpha), B.1.617.2 (Delta), and B1.427/B1.429 (Epsilon). Inoculation of eTIP1 24 h before infection reduced virus titers in lungs by two orders of magnitude (Figure 4A, *ii*, eTIP1-prophylactic). Treatment with eTIP1s 24 h post-exposure to SARS-CoV-2 also elicited protection (Figure 4A, *ii,* eTIP1-therapeutic). The protective effects of eTIP1s were lost when administered 48 h after infection, but repeating eTIP1 treatment at both 24 and 48 h post-infection increased its efficiency (Figure 5A). These results indicate that pre- and post-exposure eTIP1 prophylaxis protects from IN infection with several circulating SARS-CoV-2 variants.

Weight loss is a sensitive measure of animal distress. SARS-CoV-2 infected mice lost weight due to disease progression. Strikingly, a single IN eTIP1 dose prevented weight loss in SARS-CoV-2-infected mice. In fact, eTIP1-treated animals maintained their body weight, similar to mock-infected controls (Figure 5B). This confirmed that eTIP1s reduce SARS-CoV-2 replication and prevent disease symptoms without additional distress. Next, we wondered if eTIP1s protect lungs from SARS-CoV-2 infection-induced inflammation. Lung sections were analyzed after staining with hematoxylin and eosin (H&E) and scored on tissue pathology (Meyerholz and Beck, 2020). SARS-CoV-2-infected mice had higher histopathology scores than mock-infected mice (Figure 5C, *i* and *ii*). The major histopathology findings in infected mice were proteinaceous debris in the alveolar space, neutrophils in the interstitial space, and alveolar septal thickening. These are consistent with previous studies that detected signs of lung injury, including interstitial pneumonia, inflammatory cell infiltrates, and alveolar septal thickening (Dinnon et al., 2020; Gu et al., 2020). By histopathology analysis, treatment with eTIP1 LNPs reduced lung inflammation after exposure to SARS-CoV-2 (histopathology score of 1/16 compared to empty-LNP histopathology score of 5.4/16) at day 3 post-infection (Figure 5C, *i* and *ii*, SARS-CoV-2/eTIP1). No peribronchial inflammation was noted in the lungs when animals were treated with eTIP1s alone,

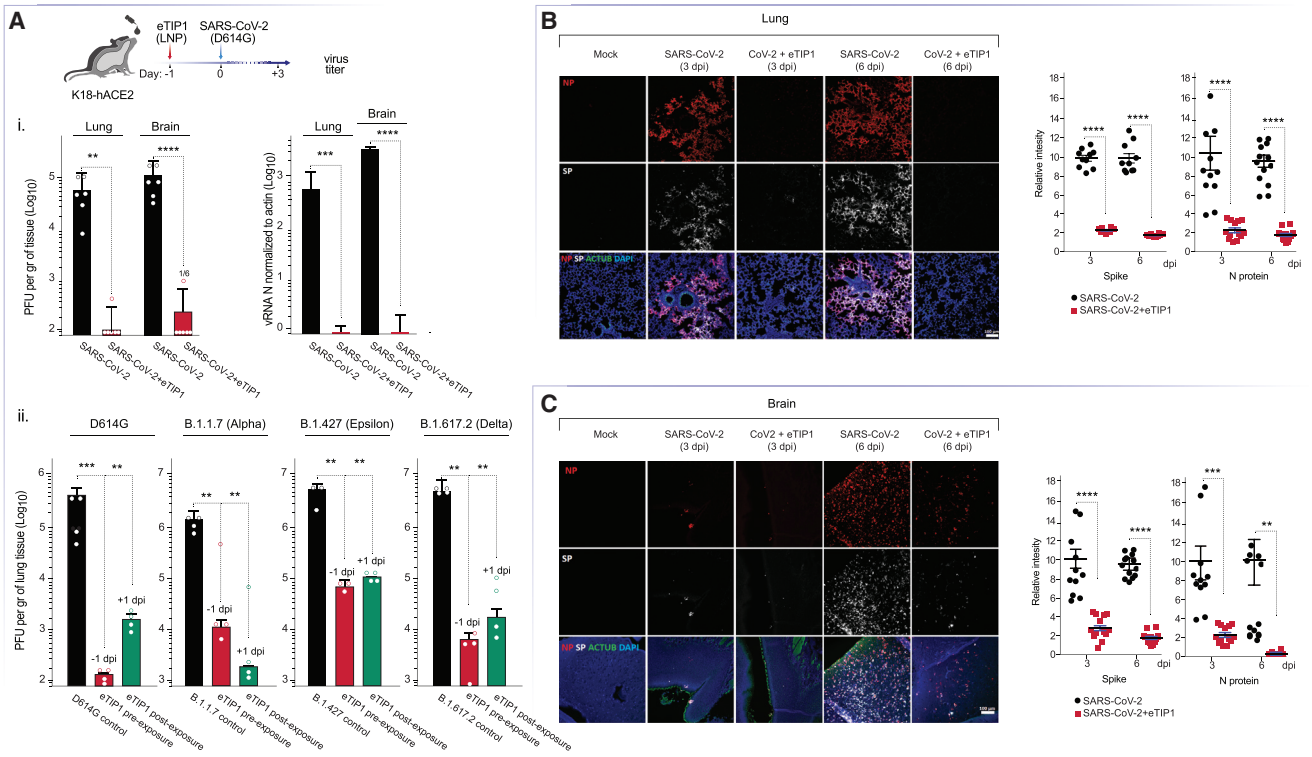

Figure 4. eTIP1 RNAs inhibit SARS-CoV-2 replication in infected mice

(A) Schematic representation of experimental design. (i) 30 μg of eTIP1 RNA/LNP or mock (empty LNP) were delivered into K18-hACE2 mice IN, and 20 h later, K18-hACE2 mice were challenged by IN inoculation 10^4 pfu SARS-CoV-2. Tissues (lung and brain) were collected at 3 days post-infection and homogenized, and supernatants were tittered by plaque assay in Vero-E6 cells. Total RNA was extracted and quantified by RT-qPCR with primers target to nucleocapsid (N) gene of SARS-CoV-2, normalized to GAPDH (n = 6). Unpaired Student's t tests. (ii) Prophylactic and therapeutic effects of eTIP1on SARS-CoV-2 variants of concerns or variants of interest (VOCs or VOIs). eTIP1 RNA/LNP was inoculated into K18-hACE2 mice by the IN route, and at 20 h post-infection, mice were infected with 10^4 pfu SARS-CoV-2 variants (D614G, B.1.1.7 [Alpha], B.1.427 [Epsilon], or B.1.617.2 [Delta]) by IN route (n = 4–5). Virus titers in lugs were determined by plaque assays.

(B and C) IHC staining for SARS-CoV-2 in lung (B) and brain (C) of infected animals. Lung and brain tissues were collected at days 3 and 6 post-infection, fixed in 4% PFA, embedded in paraffin wax, and cut into 5-μm sections. Slides were stained with antibodies that recognized SARS-CoV-2 NP (red) and spike proteins (SPs, gray). ACTUB (green), nuclear (DAPI, blue). Expression levels of SPs and NPs were qualified by Fuji/ImageJ with mean intensity and normalized to the SARS-CoV-2-infected group. For each image, we selected at least 10 areas at same places in the different groups. Unpaired Student's t tests, p values for each comparison. $^{**}p < 0.01$; $^{***}p < 0.001$; and $^{***}p < 0.001$.

indicating that eTIP1 replication does not cause persistent inflammation (Figure 5C, *i* and *ii*, eTIP1). Thus, a single IN dose of eTIP1s reduces *in vivo* replication of SARS-CoV-2 by orders of magnitude and prevents lung inflammation and SARS-CoV-2 infection-related weight loss (Jiang et al., 2020; Rappazzo et al., 2021; Sefik et al., 2021; Sun et al., 2020).

Although SARS-CoV-2 replication is strongly inhibited, H&E staining showed infiltration of lymphoid cells into the lung (Figure 5C), which may be linked to an eTIP1-mediated antiviral state. To determine which cells are recruited to the lung upon eTIP1 treatment, we performed immune cell profiling in lung tissues at 24 h after IN inoculation with eTIP1 LNPs (Figure S5). We also examined immune cell profiles 3 days post-SARS-CoV-2 infection with or without eTIP1 pre-exposure prophylaxis. No differences were observed in lung immune cell populations 24 h after inoculation with eTIP1 (Figure 5D, compare mock with eTIP1/LNPs). In the context of SARS-CoV-2 infection, eTIP1 treatment recruited different lymphoid cells into the lung, including eosinophils, plasmacytoid dendritic cells, and neutrophils, which are poorly recruited by SARS-CoV-2 infection alone (Figure 5D). Eosinophils can be recruited to the airways in response to influenza and mycobacterium tuberculosis (TB) infection in a type I IFN-dependent fashion (Bohrer et al., 2021; Samarasinghe et al., 2014). eTIP1s reduced the recruitment of CD11b+/ CD11c+/ Ly6C+ monocyte to the lungs of SARS-CoV-2-infected animals (Figure 5D), which may be associated with the pro-inflammatory response to SARS-CoV-2 infection. No other changes in immune cell populations were seen after eTIP1 pre-exposure prophylaxis (Figures 5D and S6). These data indicate that eTIP1 treatment modulates the recruitment of immune cells into the lung during SARS-CoV-2 infection.

eTIP1 treatment induces long-lasting protection against SARS-CoV-2 reinfection

A critical question is whether eTIP1-mediated protection from SARS-CoV-2 prevents the development of adaptive immunity

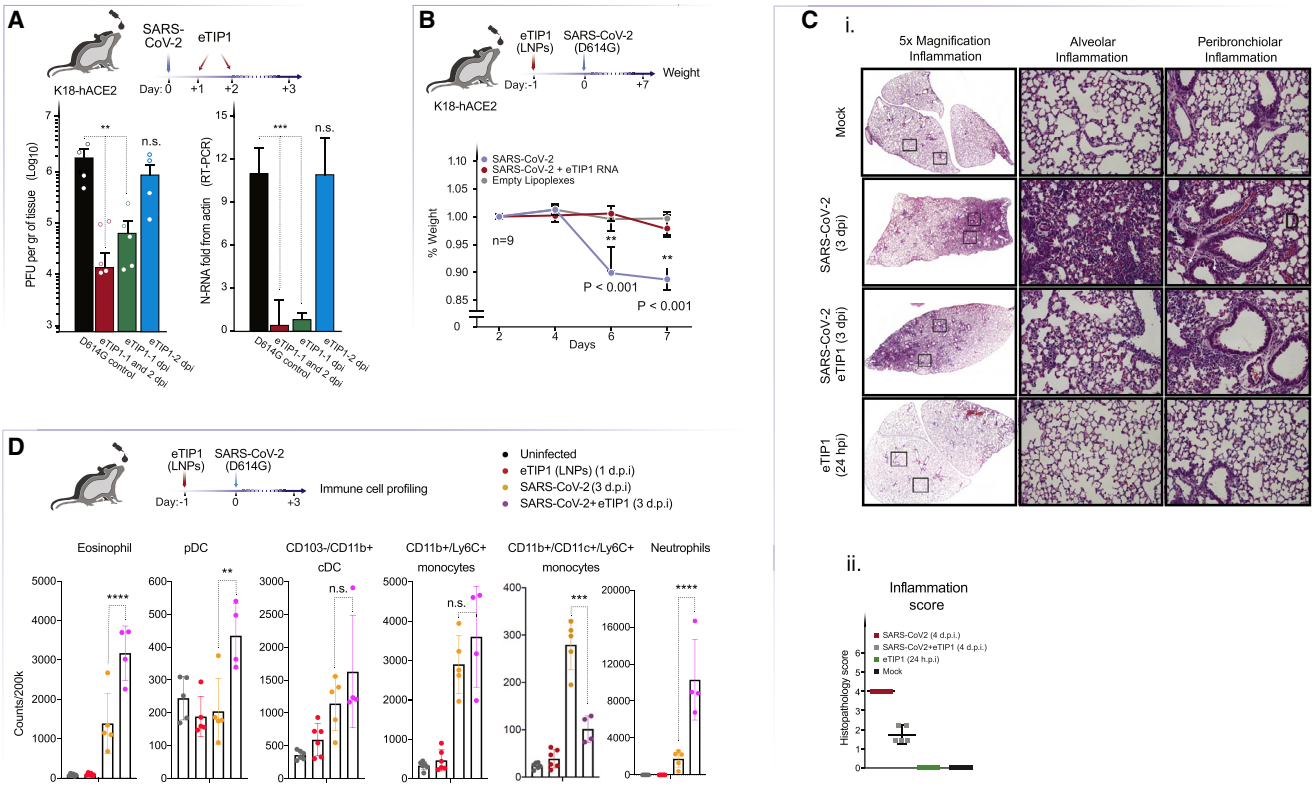

Figure 5. eTIP1 reduces the symptoms and lung damage of COVID-19 disease in infected mice by recruiting a specific set of immune cells

(A) Therapeutic window of eTIP1on SARS-CoV-2. K18-hACE2 mice were infected by the IN route with 10^4 pfu SARS-CoV-2 variants by IN route (n = 4–5). Mice were inoculated with eTIP1 RNA/LNP (30 μg) or mock (empty LNPs) at 24, 48, or 24- and 48-h post-infection. Virus titers in lungs at 3 days post-infection were determined by plaque assays.

(B) Pathogenesis, weight lost in SARS-CoV2-infected animals. Mice were treated with 30 μg of eTIP1 RNA/LNP or mock (empty LNPs) by intranasal inoculation IN, and 20 h later, K18-hACE2 mice were challenged with 10^4 pfu SARS-CoV-2. Weight changes were normalized to the initial weight for each mouse (n = 9 for each condition in two independent experiments). After animals lost 15% of their body weight, they were humanely euthanized.

(C) Lung tissues were collected at days 3 post-infection, fixed in 4% PFA, embedded in paraffin wax, and cut into 5-μm sections. Sections of lung from K18 hACE2 mice were H&E stained. Sections were evaluated for comprehensive histological changes and inflammation progression (STAR Methods).

(D) Immune cell profiling (flow cytometry) of lung of mice inoculated IN with eTIP1 RNA/LNPs (30 μg), SARS-CoV-2 infected, eTIP1 RNA/LNPs treated + SARS-CoV-2 infected or mock (empty LNPs, uninfected). Data are the number of CD45+ specific immune cells per 200,000 total cells obtained from mouse lungs (n = 3–6). Data are from two independent experiments. Unpaired Student's t tests. *p < 0.05; **p < 0.01. n.s., not significant.

against future reinfections. Immunity could last at least 5–6 months after infection (Huang et al., 2021). Thus, reinfection with SARS-CoV-2 may occur in fewer than 1% of individuals who tested positive for SARS-CoV-2, at least within 3–6 months after infection. However, the natural protection is variable and unreliable, especially among older people (Collier et al., 2021).

To test if adaptive immunity against SARS-CoV-2 is induced in animals protected by eTIP1s, mice were treated with eTIP1s or control empty LNPs, and 24 h post-treatment, mice were infected with 10^5, 10^4, or 10^3 pfu of SARS-CoV-2 (B.1.1.7 variant). Inoculation of eTIP1s reduced virus titers in lungs by three orders of magnitude more than controls (Figure 6B, for 10^5 pfu). By RT-qPCR, we found that eTIP1 treatment effectively reduced SARS-CoV-2 RNA load in lungs 24-fold compared to SARS-CoV-2 infection without eTIP1 treatment. However, we detected low levels of viral RNA in lungs (Figure 6B). At 3 weeks after infection, we measured neutralizing antibody titers. Antibody titers and seroconversion rate correlated with the initial SARS-CoV-2 concentration used to infect the mice (Figure 6C). Thus, mice infected with 10^5 pfu had a more effective induction of neutralizing antibodies than those infected with 10^4 or 10^3 pfu. Strikingly, antibody titers were similar in eTIP1-treated and untreated animals (Figure 6C). We next challenged animals intranasally with 10^5 pfu of SARS-CoV-2 (B.1.1.7) and measured virus loads in lung tissues 3 days post-reinfection (Figure 6D). Mice initially infected with 10^5 pfu of SARS-CoV-2 and treated with eTIP1 were well protected, but low doses of SARS-CoV-2 in the initial infection did not reliably generate protective immunity. Mice infected with high doses of SARS-CoV-2 were more susceptible to reinfection. Perhaps higher doses of SARS-CoV-2 suppress effective induction of adaptive immunity, enabling re-infection. Additional investigations will be necessary to fully understand this observation.

Nevertheless, our findings indicate that eTIP1s replicate in the initial infected cells at the site of administration, without spreading to other cells (Figure 3B). Given that only replication-competent

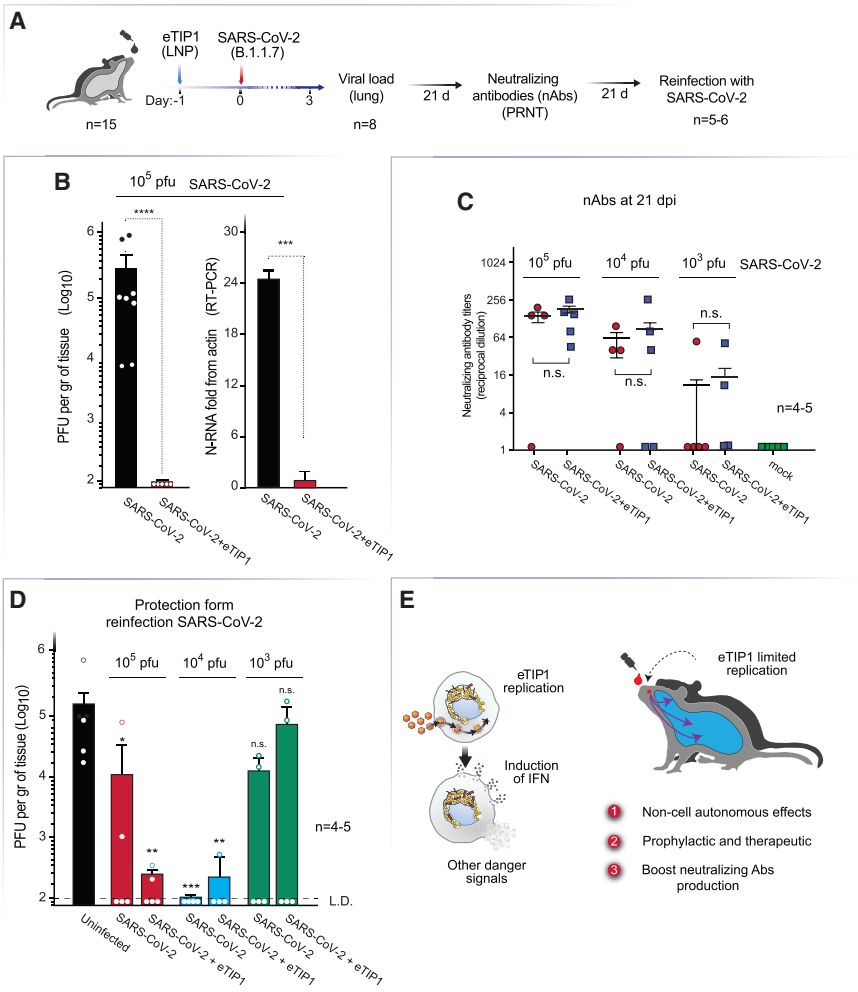

Figure 6. eTIP1 inhibits SARS-CoV-2 replication but enables the generation of neutralizing antibodies that fully protect animals from re-challenge

(A) Schematic representation of experimental design. C57BL6 mice were inoculated IN with 30 μg of eTIP1 RNA/LNP or mock inoculated (empty LNP). At 24 h after eTIP1 inoculation, mice were infected by the IN route with 10^5, 10^4, or 10^3 pfu of SARS-CoV-2 (B.1.1.7).

(B) Lung tissues were collected at 3 days post-infection and homogenized, and supernatants were tittered by plaque assay in Vero-TMPRSS2 cells. Only maximal dose 10^5 pfu is represented in the figure. Unpaired Student's t test was used for statistical analysis. ****$p < 0.0001$.

(C) At 21 days post-SARS-CoV-2 infection, mice were bled, and neutralizing antibody titers (reciprocal dilution) determined by plaque-reduction neutralizing test (PRNT). Unpaired Student's t tests. n.s., not significant.

(D) Re-infection with SARS-CoV-2. Animals that were infected with 10^5, 10^4, or 10^3 pfu of SARS-CoV-2 and recuperate or treated with eTIP1 and infected with SARS-CoV-2 (see B) were re-challenged by IN inoculation with 10^5 pfu of SARS-CoV-2 (B.1.1.7). Lung tissues were collected at 3 days post-infection and homogenized, and supernatants were tittered by plaque assay in Vero-TMPRSS2 cells. Unpaired Student's t test was used for statistical analysis. *$p < 0.03$; **$p < 0.005$; ***$p < 0.0001$. L.D. = limit of detection, 100 pfu per gram tissue.

(E) Self-replicating eTIP1 RNAs form cytosolic dsRNA intermediates and activate pattern recognition receptors, leading to the production of IFN and IFN-stimulated genes. This could also promote a protective antiviral state within the local tissue as well as at distal sites. The plasma membrane of the infected cells loses integrity and release damage-associated molecular patterns. Replication of eTIP1 within the upper-respiratory tract (red dot represents replication in nasal turbinates) send signals to recruit various types of circulating leukocytes at local (nasal-associated lymphoid tissue) and distal sites (bronchus-associated lymphoid tissue). In this way, eTIP1 can induce non-cell autonomous, distal protection, is effective prophylactically and therapeutically, and can boost neutralizing antibody production.

eTIP1s elicit protective responses (Figures 2A and S5), we hypothesize that intermediates of replication, such as dsRNA, are detected by pattern recognition receptors, leading to synthesis of type I IFN and induction of potent innate responses. Because the PV1 protease and other non-structural viral proteins in the eTIP1 induce profound rearrangements of cellular organelles and pathways, which may generate additional signals that further activate innate responses (Figure 6E). This results in the recruitment of leukocytes into the tissue and promotes an antiviral response that protects local and distal sites (non-cell-autonomous effects) (Figure 6E). Thus, molecular processes triggered by eTIP1 mimic a "natural infection" that recruits the different arms of immunity in a balanced manner, generating a protective antiviral response.

Mucosal challenges with RNA viruses achieve sterilizing immunity with no adverse effects involving short- or long-term immune dysfunction (Ascough et al., 2019; Jangra et al., 2021; Kikkert, 2020). Our data suggest that modulation of natural innate antiviral immunity is a primary component of eTIP1 antiviral activity. Importantly, a single intranasal dose prevents progression to severe viral disease longer than a single dose of small-molecule antivirals (Chen et al., 2021; Gu et al., 2020; Wang et al., 2020). We conclude that IN delivery of eTIP1 nanoparticles safely and potently stimulates host innate immunity that broadly protect from infection by reducing viral loads and preventing disease. While the antiviral response elicited by eTIP1 confers short-term protection as pre- and post-exposure prophylaxis, it does not interfere with long-term adaptive immunity (Figure 6C) that protects from reinfection (Figure 6D). We propose that eTIP1 has a compelling clinical potential in the treatment of respiratory viral disease.

DISCUSSION

Here, we provide proof of principle that DVGs can be used as pre- and post-exposure prophylaxis against diverse viral pathogens. We show that eTIP1s can be administered IN to combat respiratory infections from enterovirus to SARS-CoV-2, without

side effects. Because eTIP1 IN inoculation offers protection from 48 h before to 24 h after exposure, it provides an effective therapeutic window, comparable to small-molecule antivirals. Inoculation of eTIP1 provides rapid protection against ongoing infection, but also promotes long-term protection by generating longer-lasting adaptive immunity.

Our study provides a mechanistic rationale for decades-old observations that immunization with live attenuated PV cross-protects against other viruses and DVGs modulate the course of infection (Easton et al., 2011; Genoyer and López, 2019; Huang and Baltimore, 1970; Levi et al., 2021; Perrault and Semler, 1979; Rezelj et al., 2021; Semler et al., 1978; Vignuzzi and López, 2019). Our results are consistent with research indicating that DVG protection depends on induction of innate responses (Vignuzzi and López, 2019). For example, influenza lacking the NS1 protein was studied as a potential vaccine and antiviral approach (García-Sastre et al., 1998; Palese, 2012; Rathnasinghe et al., 2021; Zhang et al., 2018). eTIP1 treatment does not protect animals defective in type I IFN signaling (Figures 3E and S2) and offers effective protection against viruses from different families in a non-cell-autonomous manner (Figures 2, 3B, 5, and 6), in agreement with this mechanism.

In the last 2 years, the challenges of antiviral drug development have become clearer than ever. The mutational plasticity of RNA viruses can render most drug and even antibody therapies ineffective. Vaccinations, the only available tool to prevent viral infection, harness the natural defenses of the body. No similar approach is available for prophylaxis or treatment. We propose that eTIP1s provide an alternative strategy with potential benefits over conventional pharmaceuticals. While viruses can become resistant to currently available antivirals (Deng et al., 2021; Gonçalves et al., 2021; Abdool Karim and de Oliveira, 2021; Lundstrom, 2020; Zhou et al., 2021), eTIP1s induce a multicomponent antiviral response, in the form of diverse ISGs, that is unlikely to result in resistance by viral mutation. Modulation of the innate response by eTIP1 replication may enhance development of adaptive immunity, thus providing long-term protection.

Our eTIP1 design has several safety features. First, the PV backbone is non-pathogenic and can be administered non-invasively. Modification of the eTIP1 genome, based on improvements in the live-attenuated PV vaccine (Van Damme et al., 2019; Konopka-Anstadt et al., 2020; Konz et al., 2021; Yeh et al., 2020), may enhance their safety. Second, eTIP1 replication is limited to a few cells near the site of inoculation and is undetectable by 24 h (not shown). It elicits a non-cell-autonomous protective immune response without disease symptoms by recruiting immune cells that circulate throughout the respiratory tract (Figures 5D and S6). Third, because eTIP1 replicates and self-amplifies in the few cells it enters, it requires less RNA to induce full non-cell-autonomous antiviral protection. eTIP1s seem to induce a more potent responses than PV1 (Figure 3F), suggesting that the capsid proteins modulate IFN responses. Finally, the nanoparticle formulation of the eTIP1 circumvents concerns that pre-existing immunity will prevent repeated administration.

eTIP1 protective action also induces a balanced and non-detrimental antiviral state. Such a state is not seen with WT viruses, likely because all viruses evolved mechanisms to suppress antiviral responses. In addition, there was no weight loss or signs of distress in the animals treated with eTIP1s, and even those co-infected with SARS-CoV-2 showed no signs of disease. Animals infected with SARS-CoV-2 can be protected by IN administration of IFN-I (Bessière et al., 2021; Hoagland et al., 2021). However, antiviral treatments relying on administration of IFNs or dsRNA mimics (e.g., poly(I:C) or 5′triphosphate dsRNA; Caskey et al., 2011; Fitzpatrick et al., 2020; Furio et al., 2009; Gilfoy and Mason, 2007) cause side effects (e.g., fever, headache, fatigue, arthralgia, and myalgia; Channappanavar et al., 2016). We propose that eTIP1s achieve balanced regulation of innate responses and avoid the detrimental effects of IFN treatment.

One IN dose of eTIP1s provide a powerful prophylactic and therapeutic weapon in the COVID-19 pandemic and future respiratory diseases, including influenza and common cold, and other enterovirus diseases. In SARS-CoV-2 infection in mice, eTIP1s appear to thwart a proinflammatory response by SARS-CoV-2, thereby preventing damage to the lung and brain (Figure 5). The genes induced by eTIP1 are not proinflammatory but antiviral (Figures 3). Thus, eTIP1s block SARS-CoV-2 replication, an important first step in controlling disease, and redirect the host response from inflammatory to antiviral, which should increase the protection from disease. We also found that eTIP1s protect animals already infected with SARS-CoV-2 from disease and recruit immune cells, including eosinophils, plasmacytoid dendritic cells, and neutrophils (Figure 5). eTIP1 treatment reduced recruitment of myeloid subset CD11b+/ CD11c+/ Ly6C+ monocyte into the lung in infection (Figure 5D), possibly limiting production of proinflammatory cytokines. Thus, eTIP1s mediate antiviral immunity and prevent inflammation. Surprisingly, when eTIP1s are administered 24 h post-infection with SARS-CoV-2, they protect mice from infection and increase high-titer protective neutralizing antibodies (Figures 6C and 6D). We speculate that the IFN-dependent antiviral state produced by eTIP1s enhances the presentation of even small amounts of SARS-CoV-2 antigens to the adaptive immune system. eTIP1s act as an antiviral and a vaccine adjuvant, leading to short- and long-term protection.

SARS-CoV-2 infections result in heterogeneous outcomes, ranging from no symptoms to severe disease and death. The reasons are unclear. The main hypothesis is that a dysregulated immune response, probably early on, leads to systemic hyperinflammation (cytokine storm) that may drive acute respiratory distress syndrome (ARDS) and multi-organ damage in severe disease (Darif et al., 2021; Que et al., 2021; Zhou et al., 2020). Important questions are whether SARS-CoV-2 infection induces long-lasting protective immunity and if an initial infection protects from recurrent disease. In macaques, SARS-CoV-2 infection results in protective immunity when the animals are challenged soon after resolution of the primary infection (Bao et al., 2020; Chandrashekar et al., 2020; Deng et al., 2020). However, reinfection in humans has been reported a few months after initial infection, challenging the idea of long-lasting protective immunity (Cohen et al., 2021; Gupta et al., 2020; Murillo-Zamora et al., 2021). Thus, dysregulation of the immune response by SARS-CoV-2 may impair long-lasting immunity after infection. Our data suggest that eTIP1 co-infection circumvents this

limitation. eTIP1s modulate the immune response to SARS-CoV-2 infection by activating IFN-I responses (Figures 3 and 5D); this seems to counteract the suppressive effects of SARS-CoV-2, allowing production of neutralizing antibodies even if viral antigens are scarce.

We observed that differences in virus replication between eTIP1-treated and untreated animals do not change the ability of infected animals to generate protective neutralizing antibodies (Figures 6C and 6D). This suggests that the initial SARS-CoV-2 infection produces sufficient antigenic proteins to elicit protective adaptive immunity, even without SARS-CoV-2 replication and spread and that eTIP1s act as an efficient therapy against SARS-CoV-2 infection and as an adjuvant, effectively turning the infecting virus into a vaccine. We conclude that eTIP1 prevents severe disease in the short term and facilitates long-lasting adaptive immunity. This strategy may provide a solution to emerging SARS-CoV-2 variants.

Our data indicate that eTIP1s are an effective antiviral approach to harness natural immunity to fight infection in a balanced, safe, and controlled manner, utilizing the regulatory circuits that evolved to ensure protection from disease without causing self-afflicted damage (Rahim et al., 2020; Vignuzzi and López, 2019). DVG-based antiviral therapy may offer greater benefits and safety than conventional therapies, given its broad-spectrum capacity that may prevent rapid emergence of resistant variants and its short and long-lasting protective activity. These properties may contribute to fighting COVID-19 and other emerging or re-emerging viral threats.

Limitations of the study

Effective protection by eTIP1s is limited to 24–48 h before and after infection. This may reduce the usefulness of the approach to infections with a short incubation time before onset of symptoms. Our study is a proof of principle in small-animal models of infection, and more studies will be needed to understand its full therapeutic potential, given that COVID-19 characteristics are not fully replicated in mice. While we provide evidence that co-infection with a helper virus does not mobilize eTIP1 to other tissues, a more extensive trial is needed to establish the safety of this approach in the context of co-circulating enteroviruses. A particularly important question is if eTIP1 treatment can enhance disease through the induction of a ''cytokine storm'' (Fajgenbaum and June, 2020; Findlay et al., 2015; Yuan et al., 2021). The mechanisms and dynamics of the induction of protective responses are limited by the number of time points and type of samples analyzed. To optimize the efficacy and safety of this strategy, additional data with higher degrees of temporal and anatomic resolution are needed.

STAR★METHODS

Detailed methods are provided in the online version of this paper and include the following:

ACKNOWLEDGMENTS

We would like to thank Dr. Miguel Garcia-Knight for sharing SARS-CoV-2 Delta variant that he isolated in the context of clinical studies conducted in San Francisco; Drs. Luis Sigal, Eric Dang, Hiten Madhani and members of Andino lab for critical discussions and comments for manuscript preparation; and Gary Howard for editorial support. This work was supported by the DARPA INTERCEPT program managed by James Gimlett and administered through DARPA Cooperative Agreement (grant no. HR0011-17-2-0027) and NIH R41AI157129. We thank the UCSF Center for Advanced Technology core for the Illumina HiSeq4000 for RNA-seq and Gladstone Histology and Light Microscopy Core for the mouse tissue samples processing and H&E staining.

AUTHOR CONTRIBUTIONS

Y.X. designed and carried out the experiments, participated in data analysis, and wrote the manuscript. Y.S. cloned eTIP1 cDNA plasmid and generated the stable packaging cell line. G.D. developed nanostructured lipid/eTIP1 RNA complexes. C.E.G. contributed animal work and RNA-seq libraries preparation. Y.X. and P.V.L. carried out SARS-CoV-2 experiments. A.N., Y.X., and D.T. produced and purified eTIP1 particles and LNPs. Y.X. and C.T.W. carried out and analyzed the immunohistochemistry studies on tissue sections. W.S. carried out droplet RT-qPCR for gene expression analyses from tissues. Y.X., R. Aviner, and W.L. carried out RNA-seq analyses. A.C. carried out EM negative stain studies. W.Z. and J.D.E. contributed to flow cytometry analyses of lung tissues. R. Andino, J.F., R.N., J.D.E., S.B., and P.K.J. conceived and directed the project and/or wrote the manuscript.

DECLARATION OF INTERESTS

Y.X., R.N., and R. Andino have submitted a patent application. Provisional patent application: recombinant enteroviruses and uses thereof. eTIP1. US Provisional Patent Filed 7/2020. The application was accorded serial

no. 63/047,398. D.T. and R.N. are shareholders and employees of Aleph Therapeutics, Inc. E.B. is a shareholder and employee of Pine Biotech Inc.

INCLUSION AND DIVERSITY

We worked to ensure sex balance in the selection of non-human subjects. One or more of the authors of this paper self-identifies as a member of the LGBTQ+ community. One or more of the authors of this paper received support from a program designed to increase minority representation in science. While citing references scientifically relevant for this work, we also actively worked to promote gender balance in our reference list.

Received: May 11, 2021
Revised: November 8, 2021
Accepted: November 12, 2021
Published: November 18, 2021

REFERENCES

Abdool Karim, S.S., and de Oliveira, T. (2021). New SARS-CoV-2 Variants - Clinical, Public Health, and Vaccine Implications. N. Engl. J. Med. *384*, 1866–1868.

Ascough, S., Vlachantoni, I., Kalyan, M., Haijema, B.-J., Wallin-Weber, S., Dijkstra-Tiekstra, M., Ahmed, M.S., van Roosmalen, M., Grimaldi, R., Zhang, Q., et al. (2019). Local and Systemic Immunity against Respiratory Syncytial Virus Induced by a Novel Intranasal Vaccine. A Randomized, Double-Blind, Placebo-controlled Clinical Trial. Am. J. Respir. Crit. Care Med. *200*, 481–492.

Bao, L., Deng, W., Huang, B., Gao, H., Liu, J., Ren, L., Wei, Q., Yu, P., Xu, Y., Qi, F., et al. (2020). The pathogenicity of SARS-CoV-2 in hACE2 transgenic mice. Nature *583*, 830–833.

Bessière, P., Wasniewski, M., Picard-Meyer, E., Servat, A., Figueroa, T., Foret-Lucas, C., Coggon, A., Lesellier, S., Boué, F., Cebron, N., et al. (2021). Intranasal type I interferon treatment is beneficial only when administered before clinical signs onset in the SARS-CoV-2 hamster model. PLoS Pathog. *17*, e1009427.

Bohrer, A.C., Castro, E., Hu, Z., Queiroz, A.T.L., Tocheny, C.E., Assmann, M., Sakai, S., Nelson, C., Baker, P.J., Ma, H., et al.; Tuberculosis Imaging Program (2021). Eosinophils are part of the granulocyte response in tuberculosis and promote host resistance in mice. J. Exp. Med. *218*, e20210469.

Brennan, K., and Bowie, A.G. (2010). Activation of host pattern recognition receptors by viruses. Curr. Opin. Microbiol. *13*, 503–507.

Burrill, C.P., Strings, V.R., and Andino, R. (2013a). Poliovirus: Generation, Quantification, Propagation, Purification, and Storage. Curr. Protoc. Microbiol. https://doi.org/10.1002/9780471729259.mc15h01s29.

Burrill, C.P., Strings, V.R., Schulte, M.B., and Andino, R. (2013b). Poliovirus: Generation and Characterization of Mutants. Curr. Protoc. Microbiol. https://doi.org/10.1002/9780471729259.mc15h02s29.

Canedo-Marroquín, G., Saavedra, F., Andrade, C.A., Berrios, R.V., Rodríguez-Guilarte, L., Opazo, M.C., Riedel, C.A., and Kalergis, A.M. (2020). SARS-CoV-2: Immune Response Elicited by Infection and Development of Vaccines and Treatments. Front. Immunol. *11*, 569760.

Caskey, M., Lefebvre, F., Filali-Mouhim, A., Cameron, M.J., Goulet, J.-P., Haddad, E.K., Breton, G., Trumpfheller, C., Pollak, S., Shimeliovich, I., et al. (2011). Synthetic double-stranded RNA induces innate immune responses similar to a live viral vaccine in humans. J. Exp. Med. *208*, 2357–2366.

Chandrashekar, A., Liu, J., Martinot, A.J., McMahan, K., Mercado, N.B., Peter, L., Tostanoski, L.H., Yu, J., Maliga, Z., Nekorchuk, M., et al. (2020). SARS-CoV-2 infection protects against rechallenge in rhesus macaques. Science *369*, 812–817.

Channappanavar, R., Fehr, A.R., Vijay, R., Mack, M., Zhao, J., Meyerholz, D.K., and Perlman, S. (2016). Dysregulated Type I Interferon and Inflammatory Monocyte-Macrophage Responses Cause Lethal Pneumonia in SARS-CoV-Infected Mice. Cell Host Microbe *19*, 181–193.

Chen, R.E., Winkler, E.S., Case, J.B., Aziati, I.D., Bricker, T.L., Joshi, A., Darling, T.L., Ying, B., Errico, J.M., Shrihari, S., et al. (2021). In vivo monoclonal antibody efficacy against SARS-CoV-2 variant strains. Nature *596*, 103–108.

Chumakov, K.M., Powers, L.B., Noonan, K.E., Roninson, I.B., and Levenbook, I.S. (1991). Correlation between amount of virus with altered nucleotide sequence and the monkey test for acceptability of oral poliovirus vaccine. Proc. Natl. Acad. Sci. USA *88*, 199–203.

Chumakov, K., Benn, C.S., Aaby, P., Kottilil, S., and Gallo, R. (2020). Can existing live vaccines prevent COVID-19? Science *368*, 1187–1188.

Cohen, C., Kleynhans, J., Gottberg, A., von, McMorrow, M.L., Wolter, N., Bhiman, J.N., Moyes, J., Plessis, M., du, Carrim, M., Buys, A., et al. (2021). SARS-CoV-2 incidence, transmission and reinfection in a rural and an urban setting: results of the PHIRST-C cohort study, South Africa, 2020-2021. Medrxiv. https://doi.org/10.1101/2021.07.20.21260855.

Collier, D.A., Ferreira, I.A.T.M., Kotagiri, P., Datir, R.P., Lim, E.Y., Touizer, E., Meng, B., Abdullahi, A., Elmer, A., Kingston, N., et al.; CITIID-NIHR BioResource COVID-19 Collaboration (2021). Age-related immune response heterogeneity to SARS-CoV-2 vaccine BNT162b2. Nature *596*, 417–422.

Crotty, S., and Andino, R. (2002). Implications of high RNA virus mutation rates: lethal mutagenesis and the antiviral drug ribavirin. Microbes Infect. *4*, 1301–1307.

Crotty, S., Cameron, C.E., and Andino, R. (2001). RNA virus error catastrophe: direct molecular test by using ribavirin. Proc. Natl. Acad. Sci. USA *98*, 6895–6900.

Darif, D., Hammi, I., Kihel, A., El Idrissi Saik, I., Guessous, F., and Akarid, K. (2021). The pro-inflammatory cytokines in COVID-19 pathogenesis: What goes wrong? Microb. Pathog. *153*, 104799.

Deng, W., Bao, L., Liu, J., Xiao, C., Liu, J., Xue, J., Lv, Q., Qi, F., Gao, H., Yu, P., et al. (2020). Primary exposure to SARS-CoV-2 protects against reinfection in rhesus macaques. Science *369*, 818–823.

Deng, X., Garcia-Knight, M.A., Khalid, M.M., Servellita, V., Wang, C., Morris, M.K., Sotomayor-González, A., Glasner, D.R., Reyes, K.R., Gliwa, A.S., et al. (2021). Transmission, infectivity, and neutralization of a spike L452R SARS-CoV-2 variant. Cell *184*, 3426–3437.e8.

Dimmock, N.J., and Easton, A.J. (2014). Defective interfering influenza virus RNAs: time to reevaluate their clinical potential as broad-spectrum antivirals? J. Virol. *88*, 5217–5227.

Dimmock, N.J., and Easton, A.J. (2015). Cloned Defective Interfering Influenza RNA and a Possible Pan-Specific Treatment of Respiratory Virus Diseases. Viruses *7*, 3768–3788.

Dinnon, K.H., 3rd, Leist, S.R., Schäfer, A., Edwards, C.E., Martinez, D.R., Montgomery, S.A., West, A., Yount, B.L., Jr., Hou, Y.J., Adams, L.E., et al. (2020). A mouse-adapted model of SARS-CoV-2 to test COVID-19 countermeasures. Nature *586*, 560–566.

Domingo, E., Escarmís, C., Sevilla, N., Moya, A., Elena, S.F., Quer, J., Novella, I.S., and Holland, J.J. (1996). Basic concepts in RNA virus evolution. FASEB J. *10*, 859–864.

Domingo, E., Ruiz-Jarabo, C.M., Sierra, S., Arias, A., Pariente, N., Baranowski, E., and Escarmis, C. (2002). Emergence and selection of RNA virus variants: memory and extinction. Virus Res. *82*, 39–44.

Easton, A.J., Scott, P.D., Edworthy, N.L., Meng, B., Marriott, A.C., and Dimmock, N.J. (2011). A novel broad-spectrum treatment for respiratory virus infections: influenza-based defective interfering virus provides protection against pneumovirus infection in vivo. Vaccine *29*, 2777–2784.

Fajgenbaum, D.C., and June, C.H. (2020). Cytokine Storm. N. Engl. J. Med. *383*, 2255–2273.

Findlay, J.S., Ulaeto, D., and D'Elia, R.V. (2015). Cytokines and viral hemorrhagic fever: potential for therapeutic intervention. Future Virology *5*, 547–557.

Finlay, B.B., and McFadden, G. (2006). Anti-immunology: evasion of the host immune system by bacterial and viral pathogens. Cell *124*, 767–782.

Fitzpatrick, J.-M., Minogue, E., Curham, L., Tyrrell, H., Gavigan, P., Hind, W., and Downer, E.J. (2020). MyD88-dependent and -independent signalling via TLR3 and TLR4 are differentially modulated by Δ^9-tetrahydrocannabinol and cannabidiol in human macrophages. J. Neuroimmunol. *343*, 577217.

Furio, L., Billard, H., Valladeau, J., Péguet-Navarro, J., and Berthier-Vergnes, O. (2009). Poly(I:C)-Treated human langerhans cells promote the differentiation of CD4+ T cells producing IFN-γ and IL-10. J. Invest. Dermatol. *129*, 1963–1971.

García-Sastre, A., Egorov, A., Matassov, D., Brandt, S., Levy, D.E., Durbin, J.E., Palese, P., and Muster, T. (1998). Influenza A virus lacking the NS1 gene replicates in interferon-deficient systems. Virology *252*, 324–330.

Geller, R., Taguwa, S., and Frydman, J. (2012). Broad action of Hsp90 as a host chaperone required for viral replication. Biochim. Biophys. Acta *1823*, 698–706.

Genoyer, E., and López, C.B. (2019). The Impact of Defective Viruses on Infection and Immunity. Annu. Rev. Virol. *6*, 547–566.

Gilfoy, F.D., and Mason, P.W. (2007). West Nile virus-induced interferon production is mediated by the double-stranded RNA-dependent protein kinase PKR. J. Virol. *81*, 11148–11158.

Goff, P.H., Gao, Q., and Palese, P. (2012). A majority of infectious Newcastle disease virus particles contain a single genome, while a minority contain multiple genomes. J. Virol. *86*, 10852–10856.

Gonçalves, B.C., Lopes Barbosa, M.G., Silva Olak, A.P., Belebecha Terezo, N., Nishi, L., Watanabe, M.A., Marinello, P., Zendrini Rechenchoski, D., Dejato Rocha, S.P., and Faccin-Galhardi, L.C. (2021). Antiviral therapies: advances and perspectives. Fundam. Clin. Pharmacol. *35*, 305–320.

Gu, H., Chen, Q., Yang, G., He, L., Fan, H., Deng, Y.-Q., Wang, Y., Teng, Y., Zhao, Z., Cui, Y., et al. (2020). Adaptation of SARS-CoV-2 in BALB/c mice for testing vaccine efficacy. Science *369*, 1603–1607.

Guo, K., Barrett, B.S., Mickens, K.L., Hasenkrug, K.J., and Santiago, M.L. (2021). Interferon Resistance of Emerging SARS-CoV-2 Variants. BioRxiv. https://doi.org/10.1101/2021.03.20.436257.

Gupta, V., Bhoyar, R.C., Jain, A., Srivastava, S., Upadhayay, R., Imran, M., Jolly, B., Divakar, M.K., Sharma, D., Sehgal, P., et al. (2020). Asymptomatic Reinfection in 2 Healthcare Workers From India With Genetically Distinct Severe Acute Respiratory Syndrome Coronavirus 2. Clin. Infect. Dis. *73*, e2823–e2825.

Hoagland, D.A., Møller, R., Uhl, S.A., Oishi, K., Frere, J., Golynker, I., Horiuchi, S., Panis, M., Blanco-Melo, D., Sachs, D., et al. (2021). Leveraging the antiviral type I interferon system as a first line of defense against SARS-CoV-2 pathogenicity. Immunity *54*, 557–570.e5.

Huang, A.S., and Baltimore, D. (1970). Defective viral particles and viral disease processes. Nature *226*, 325–327.

Huang, Q., Ji, K., Tian, S., Wang, F., Huang, B., Tong, Z., Tan, S., Hao, J., Wang, Q., Tan, W., et al. (2021). A single-dose mRNA vaccine provides a long-term protection for hACE2 transgenic mice from SARS-CoV-2. Nat. Commun. *12*, 776.

Ida-Hosonuma, M., Iwasaki, T., Yoshikawa, T., Nagata, N., Sato, Y., Sata, T., Yoneyama, M., Fujita, T., Taya, C., Yonekawa, H., and Koike, S. (2005). The alpha/beta interferon response controls tissue tropism and pathogenicity of poliovirus. J. Virol. *79*, 4460–4469.

Jangra, S., De Vrieze, J., Choi, A., Rathnasinghe, R., Laghlali, G., Uvyn, A., Van Herck, S., Nuhn, L., Deswarte, K., Zhong, Z., et al. (2021). Sterilizing Immunity against SARS-CoV-2 Infection in Mice by a Single-Shot and Lipid Amphiphile Imidazoquinoline TLR7/8 Agonist-Adjuvanted Recombinant Spike Protein Vaccine*. Angew. Chem. Int. Ed. Engl. *60*, 9467–9473.

Jiang, R.-D., Liu, M.-Q., Chen, Y., Shan, C., Zhou, Y.-W., Shen, X.-R., Li, Q., Zhang, L., Zhu, Y., Si, H.-R., et al. (2020). Pathogenesis of SARS-CoV-2 in Transgenic Mice Expressing Human Angiotensin-Converting Enzyme 2. Cell *182*, 50–58.e8.

Kang, L., He, G., Sharp, A.K., Wang, X., Brown, A.M., Michalak, P., and Weger-Lucarelli, J. (2021). A selective sweep in the Spike gene has driven SARS-CoV-2 human adaptation. Cell *184*, 4392–4400.e4.

Kikkert, M. (2020). Innate Immune Evasion by Human Respiratory RNA Viruses. J. Innate Immun. *12*, 4–20.

Kim, K.H., Narayanan, K., and Makino, S. (1998). Characterization of coronavirus DI RNA packaging. Adv. Exp. Med. Biol. *440*, 347–353.

Kitamura, N., Semler, B.L., Rothberg, P.G., Larsen, G.R., Adler, C.J., Dorner, A.J., Emini, E.A., Hanecak, R., Lee, J.J., van der Werf, S., et al. (1981). Primary structure, gene organization and polypeptide expression of poliovirus RNA. Nature *291*, 547–553.

Konopka-Anstadt, J.L., Campagnoli, R., Vincent, A., Shaw, J., Wei, L., Wynn, N.T., Smithee, S.E., Bujaki, E., Te Yeh, M., Laassri, M., et al. (2020). Development of a new oral poliovirus vaccine for the eradication end game using codon deoptimization. NPJ Vaccines *5*, 26.

Konz, J.O., Schofield, T., Carlyle, S., Wahid, R., Ansari, A., Strating, J.R.P.M., Yeh, M.T., Manukyan, H., Smits, S.L., Tritama, E., et al. (2021). Evaluation and validation of next-generation sequencing to support lot release for a novel type 2 oral poliovirus vaccine. Vaccine X *8*, 100102.

Kranz, L.M., Diken, M., Haas, H., Kreiter, S., Loquai, C., Reuter, K.C., Meng, M., Fritz, D., Vascotto, F., Hefesha, H., et al. (2016). Systemic RNA delivery to dendritic cells exploits antiviral defence for cancer immunotherapy. Nature *534*, 396–401.

Levi, L.I., Rezelj, V.V., Henrion-Lacritick, A., Erazo, D., Boussier, J., Vallet, T., Bernhauerová, V., Suzuki, Y., Carrau, L., Weger-Lucarelli, J., et al. (2021). Defective viral genomes from chikungunya virus are broad-spectrum antivirals and prevent virus dissemination in mosquitoes. PLoS Pathog. *17*, e1009110.

Li, D., Wei, J., Yang, F., Liu, H.-N., Zhu, Z.-X., Cao, W.-J., Li, S., Liu, X.-T., Zheng, H.-X., and Shu, H.-B. (2016a). Foot-and-mouth disease virus structural protein VP3 degrades Janus kinase 1 to inhibit IFN-γ signal transduction pathways. Cell Cycle *15*, 850–860.

Li, D., Yang, W., Yang, F., Liu, H., Zhu, Z., Lian, K., Lei, C., Li, S., Liu, X., Zheng, H., and Shu, H. (2016b). The VP3 structural protein of foot-and-mouth disease virus inhibits the IFN-β signaling pathway. FASEB J. *30*, 1757–1766.

Lundstrom, K. (2020). Coronavirus Pandemic-Therapy and Vaccines. Biomedicines *8*, 109.

Lutrick, K., Ellingson, K.D., Baccam, Z., Rivers, P., Beitel, S., Parker, J., Hollister, J., Sun, X., Gerald, J.K., Komatsu, K., et al. (2021). COVID-19 Infection, Reinfection, and Vaccine Effectiveness in a Prospective Cohort of Arizona Frontline/Essential Workers: The AZ HEROES Research Protocol. JMIR Res Protoc. *10*, e28925.

McClure, M.A., Holland, J.J., and Perrault, J. (1980). Generation of defective interfering particles in picornaviruses. Virology *100*, 408–418.

Meganck, R.M., and Baric, R.S. (2021). Developing therapeutic approaches for twenty-first-century emerging infectious viral diseases. Nat. Med. *27*, 401–410.

Meyerholz, D.K., and Beck, A.P. (2020). Histopathologic Evaluation and Scoring of Viral Lung Infection. Methods Mol. Biol. *2099*, 205–220.

Murillo-Zamora, E., Mendoza-Cano, O., Delgado-Enciso, I., and Hernandez-Suarez, C.M. (2021). Predictors of severe symptomatic laboratory-confirmed SARS-CoV-2 reinfection. Public Health *193*, 113–115.

Narayanan, K., and Makino, S. (2009). Coronaviruses and arteriviruses. In Cellular Signaling and Innate Immune Responses to RNA Virus Infections. A.R. Brasier, A. García-Sastre, S.M. Lemon, eds. (ASM Press). pp. 373–387.

Nagata, N., Iwasaki, T., Ami, Y., Sato, Y., Hatano, I., Harashima, A., Suzaki, Y., Yoshii, T., Hashikawa, T., Sata, T., et al. (2004). A poliomyelitis model through mucosal infection in transgenic mice bearing human poliovirus receptor, TgPVR21. Virology *321*, 87–100.

Nelemans, T., and Kikkert, M. (2019). Viral Innate Immune Evasion and the Pathogenesis of Emerging RNA Virus Infections. Viruses *11*, 961.

Ohka, S., Igarashi, H., Nagata, N., Sakai, M., Koike, S., Nochi, T., Kiyono, H., and Nomoto, A. (2007). Establishment of a poliovirus oral infection system in

human poliovirus receptor-expressing transgenic mice that are deficient in alpha/beta interferon receptor. J. Virol. *81*, 7902–7912.

Palese, P. (2012). 128 Toward a Universal Influenza Virus Vaccine. JAIDS Journal of Acquired Immune Deficiency Syndromes *59*, 53.

Peersen, O.B. (2017). Picornaviral polymerase structure, function, and fidelity modulation. Virus Res. *234*, 4–20.

Perrault, J. (1981). Origin and Replication of Defective Interfering Particles. In Current Topics in Microbiology and Immunology: Initiation Signals in Viral Gene Expression (Springer), pp. 151–207.

Perrault, J., and Semler, B.L. (1979). Internal genome deletions in two distinct classes of defective interfering particles of vesicular stomatitis virus. Proc. Natl. Acad. Sci. USA *76*, 6191–6195.

Pfeiffer, J.K. (2010). Innate host barriers to viral trafficking and population diversity: lessons learned from poliovirus. Adv. Virus Res. *77*, 85–118.

Pfeiffer, J.K., and Kirkegaard, K. (2003). A single mutation in poliovirus RNA-dependent RNA polymerase confers resistance to mutagenic nucleotide analogs via increased fidelity. Proc. Natl. Acad. Sci. USA *100*, 7289–7294.

Preissner, K.T., Fischer, S., and Deindl, E. (2020). Extracellular RNA as a Versatile DAMP and Alarm Signal That Influences Leukocyte Recruitment in Inflammation and Infection. Front. Cell Dev. Biol. *8*, 619221.

Que, Y., Hu, C., Wan, K., Hu, P., Wang, R., Luo, J., Li, T., Ping, R., Hu, Q., Sun, Y., et al. (2021). Cytokine release syndrome in COVID-19: a major mechanism of morbidity and mortality. Int. Rev. Immunol. https://doi.org/10.1080/08830185.2021.1884248.

Rahim, M.M.A., Parsons, B.D., Price, E.L., Slaine, P.D., Chilvers, B.L., Seaton, G.S., Wight, A., Medina-Luna, D., Dey, S., Grandy, S.L., et al. (2020). Defective Influenza A Virus RNA Products Mediate MAVS-Dependent Upregulation of Human Leukocyte Antigen Class I Proteins. J. Virol. *94*, e00165-20.

Rappazzo, C.G., Tse, L.V., Kaku, C.I., Wrapp, D., Sakharkar, M., Huang, D., Deveau, L.M., Yockachonis, T.J., Herbert, A.S., Battles, M.B., et al. (2021). Broad and potent activity against SARS-like viruses by an engineered human monoclonal antibody. Science *371*, 823–829.

Rathnasinghe, R., Salvatore, M., Zheng, H., Jangra, S., Kehrer, T., Mena, I., Schotsaert, M., Muster, T., Palese, P., and García-Sastre, A. (2021). Prophylactic protection against respiratory viruses conferred by a prototype live attenuated influenza virus vaccine. BioRxiv. https://doi.org/10.1101/2021.04.28.441797.

Rezelj, V.V., Carrau, L., Merwaiss, F., Levi, L.I., Erazo, D., Tran, Q.D., Henrion-Lacritick, A., Gausson, V., Suzuki, Y., Shengjuler, D., et al. (2021). Defective viral genomes as therapeutic interfering particles against flavivirus infection in mammalian and mosquito hosts. Nat. Commun. *12*, 2290.

Samarasinghe, A.E., Woolard, S.N., Boyd, K.L., Hoselton, S.A., Schuh, J.M., and McCullers, J.A. (2014). The immune profile associated with acute allergic asthma accelerates clearance of influenza virus. Immunol. Cell Biol. *92*, 449–459.

Scheideler, M., Vidakovic, I., and Prassl, R. (2020). Lipid nanocarriers for microRNA delivery. Chem. Phys. Lipids *226*, 104837.

Schoggins, J.W., and Rice, C.M. (2011). Interferon-stimulated genes and their antiviral effector functions. Curr. Opin. Virol. *1*, 519–525.

Schoggins, J.W., Wilson, S.J., Panis, M., Murphy, M.Y., Jones, C.T., Bieniasz, P., and Rice, C.M. (2011). A diverse range of gene products are effectors of the type I interferon antiviral response. Nature *472*, 481–485.

Schoggins, J.W., MacDuff, D.A., Imanaka, N., Gainey, M.D., Shrestha, B., Eitson, J.L., Mar, K.B., Richardson, R.B., Ratushny, A.V., Litvak, V., et al. (2014). Pan-viral specificity of IFN-induced genes reveals new roles for cGAS in innate immunity. Nature *505*, 691–695.

Sefik, E., Israelow, B., Zhao, J., Qu, R., Song, E., Mirza, H., Kaffe, E., Halene, S., Meffre, E., Kluger, Y., et al. (2021). A humanized mouse model of chronic COVID-19 to evaluate disease mechanisms and treatment options (Res Square).

Semler, B.L., Perrault, J., Abelson, J., and Holland, J.J. (1978). Sequence of a RNA templated by the 3′-OH RNA terminus of defective interfering particles of vesicular stomatitis virus. Proc. Natl. Acad. Sci. USA *75*, 4704–4708.

Shirogane, Y., Rousseau, E., Voznica, J., Rouzine, I.M., Bianco, S., and Andino, R. (2019). Experimental and mathematical insights on the competition between poliovirus and a defective interfering genome. bioRxiv. https://doi.org/10.1101/519751.

Shirogane, Y., Rousseau, E., Voznica, J., Xiao, Y., Su, W., Catching, A., Whitfield, Z.J., Rouzine, I.M., Bianco, S., and Andino, R. (2021a). Experimental and mathematical insights on the interactions between poliovirus and a defective interfering genome. BioRxiv. https://doi.org/10.1101/2021.01.11.426198.

Shirogane, Y., Rousseau, E., Voznica, J., Xiao, Y., Su, W., Catching, A., Whitfield, Z.J., Rouzine, I.M., Bianco, S., and Andino, R. (2021b). Experimental and mathematical insights on the interactions between poliovirus and a defective interfering genome. PLoS Pathog. *17*, e1009277.

Sun, S.-H., Chen, Q., Gu, H.-J., Yang, G., Wang, Y.-X., Huang, X.-Y., Liu, S.-S., Zhang, N.-N., Li, X.-F., Xiong, R., et al. (2020). A Mouse Model of SARS-CoV-2 Infection and Pathogenesis. Cell Host Microbe *28*, 124–133.e4.

Sun, Z., Kim, A., Sobolewski, M.D., Enick, N., Chen, C., Adams, C., Jacobs, J.L., McCormick, K.D., Mellors, J.W., Dimitrov, D.S., and Li, W. (2021). Neutralization of European, South African, and United States SARS-CoV-2 mutants by a human antibody and antibody domains. BioRxiv. https://doi.org/10.1101/2021.03.22.436481.

Trapnell, C., Roberts, A., Goff, L., Pertea, G., Kim, D., Kelley, D.R., Pimentel, H., Salzberg, S.L., Rinn, J.L., and Pachter, L. (2012). Differential gene and transcript expression analysis of RNA-seq experiments with TopHat and Cufflinks. Nat. Protoc. *7*, 562–578.

Tse, L.V., Meganck, R.M., Graham, R.L., and Baric, R.S. (2020). The Current and Future State of Vaccines, Antivirals and Gene Therapies Against Emerging Coronaviruses. Front. Microbiol. *11*, 658.

Van Damme, P., De Coster, I., Bandyopadhyay, A.S., Revets, H., Withanage, K., De Smedt, P., Suykens, L., Oberste, M.S., Weldon, W.C., Costa-Clemens, S.A., et al. (2019). The safety and immunogenicity of two novel live attenuated monovalent (serotype 2) oral poliovirus vaccines in healthy adults: a double-blind, single-centre phase 1 study. Lancet *394*, 148–158.

Vignuzzi, M., and López, C.B. (2019). Defective viral genomes are key drivers of the virus-host interaction. Nat. Microbiol. *4*, 1075–1087.

Wang, C., Li, W., Drabek, D., Okba, N.M.A., van Haperen, R., Osterhaus, A.D.M.E., van Kuppeveld, F.J.M., Haagmans, B.L., Grosveld, F., and Bosch, B.-J. (2020). A human monoclonal antibody blocking SARS-CoV-2 infection. Nat. Commun. *11*, 2251.

White, K.M., Rosales, R., Yildiz, S., Kehrer, T., Miorin, L., Moreno, E., Jangra, S., Uccellini, M.B., Rathnasinghe, R., and Coughlan, L. (2021). Plitidepsin has potent preclinical efficacy against SARS-CoV-2 by targeting the host protein eEF1A. Science *371*, 926–931.

WHO (2021). Coronavirus diseas (COVID-19). https://www.who.int/health-topics/coronavirus#tab=tab_1.

Winkler, E.S., Bailey, A.L., Kafai, N.M., Nair, S., McCune, B.T., Yu, J., Fox, J.M., Chen, R.E., Earnest, J.T., Keeler, S.P., et al. (2020). SARS-CoV-2 infection of human ACE2-transgenic mice causes severe lung inflammation and impaired function. Nat. Immunol. *21*, 1327–1335.

Xiao, Y., Dolan, P.T., Goldstein, E.F., Li, M., Farkov, M., Brodsky, L., and Andino, R. (2017). Poliovirus intrahost evolution is required to overcome tissue-specific innate immune responses. Nat. Commun. *8*, 375.

Yeh, M.T., Bujaki, E., Dolan, P.T., Smith, M., Wahid, R., Konz, J., Weiner, A.J., Bandyopadhyay, A.S., Van Damme, P., De Coster, I., et al. (2020). Engineering the Live-Attenuated Polio Vaccine to Prevent Reversion to Virulence. Cell Host Microbe *27*, 736–751.e8.

Zhang, L., Wang, J., Muñoz-Moreno, R., Kim, M., Sakthivel, R., Mo, W., Shao, D., Anantharaman, A., García-Sastre, A., Conrad, N.K., et al. (2018). Influenza Virus NS1 Protein RNA-Interactome Reveals Intron Targeting. J. Virol. *92*, e01634-18.

Yuan, S., Jiang, S.-C., Zhang, Z.-W., Fu, Y.-F., Hu, J., and Li, Z.-L. (2021). Quantification of Cytokine Storms During Virus Infections. Front. Immunol. *12*, 659419.

Zhang, J., Ding, N., Song, Y., Song, R., Pan, Y., Wang, L., Yan, S., Wang, Q., Ma, S., Wei, L., et al. (2021). Phylogenomic tracing of asymptomatic transmission in a COVID-19 outbreak. Innovation *2*, 100099.

Zhou, F., Yu, T., Du, R., Fan, G., Liu, Y., Liu, Z., Xiang, J., Wang, Y., Song, B., Gu, X., et al. (2020). Clinical course and risk factors for mortality of adult inpatients with COVID-19 in Wuhan, China: a retrospective cohort study. Lancet *395*, 1054–1062.

Zhou, B., Thao, T.T.N., Hoffmann, D., Taddeo, A., Ebert, N., Labroussaa, F., Pohlmann, A., King, J., Steiner, S., Kelly, J.N., et al. (2021). SARS-CoV-2 spike D614G change enhances replication and transmission. Nature *592*, 122–127.

Zhu, N., Zhang, D., Wang, W., Li, X., Yang, B., Song, J., Zhao, X., Huang, B., Shi, W., Lu, R., et al.; China Novel Coronavirus Investigating and Research Team (2020). A Novel Coronavirus from Patients with Pneumonia in China, 2019. N. Engl. J. Med. *382*, 727–733.

STAR★METHODS

KEY RESOURCES TABLE

REAGENT or RESOURCE	SOURCE	IDENTIFIER
Antibodies		
CD45	Biolegend	Cat#103128, RRID#AB_493715
CD11c	Biolegend	Cat#117324, RRID#AB_830649
Singlec-F	BD Biosciences	Cat#552126, RRID: AB_394341
Ly6G	Biolegend	Cat#127618, RRID: AB_1877261
Ly6C	Biolegend	Cat#128036, RRID: AB_2562353
CD11b	Biolegend	Cat#101242,RRID: AB_2563310
CD103	Biolegend	Cat#121414,RRID: AB_1227502
MHC-2	Biolegend	Cat#107632, RRID: AB_2650896
CD45R	Biolegend	Cat#103210, RRID: AB_312995
CD317	Biolegend	Cat#127012, RRID: AB_1953287
eFluor 506 Fix Viability	eBioscience	Cat#65-0866-14
NK1.1	Biolegend	Cat#156508, RRID: AB_2876526
CD19	Biolegend	Cat#115508, RRID: AB_313643
CD3	Biolegend	Cat#100214, RRID: AB_493645
GammaDeltaTCR	Biolegend	Cat#118129, RRID: AB_2563356
CD4	Biolegend	Cat#100412,RRID: AB_312697
CD8a	Biolegend	Cat#100722, RRID: AB_312761
Mouse Fc block	BD PharMingen	Cat#553141, RRID: AB_394656
BD brilliant stain buffer	BD Biosciences	Cat#563794, RRID: AB_2869761
anti-acetylated α Tubulin (ACTUB)	Santa Cruz	Cat#sc-23950, clone: 6-11B-1
anti-SARS-CoV-2 nucleocapsid(N)	GeneTex	Cat#GTX135361, RRID: AB_2887484
anti-SARS-CoV-2 spike(S)	GeneTex	Cat#GTX632604, RRID: AB_2864418
Polio-3A antibody	This paper	N/A
Polio-3B-Vpg antibody	This paper	N/A
Bacterial and virus strains		
SARS-CoV-2, USA-WA1/2020	BEI	Cat No: NR-52281
SARS-CoV-2, D614G	A Gift from Sara Sunshine, (UCSF)	N/A
SARS-CoV-2, B1.4.27	A gift from Charles Chiu lab(UCSF)	N/A
SARS-CoV-2, B1.1.7	This paper	N/A
SARS-CoV-2, B.1.617.2	This paper	N/A
PV1	This paper	N/A
CVB3	This paper	N/A
EV-71	This paper	N/A
EV-D68	This paper	N/A
Rhinovirus 16, 1B	This paper	N/A
Influenza A H1N1(PR8 strain)	A gift from the Professor Christopher Byron Brooke (University of Illinois)	N/A
Chemicals, peptides, and recombinant proteins		
Dulbecco's Modified Eagle's Medium	Sigma-Aldrich	Cat#D5796
Bovine albumin fraction V, 7.5%	GIBCO	Cat#15260037
Formaldehyde solution	Sigma	Cat#252549
Crystal violet	Sigma	Cat#C0775
RPIM-1640	GIBCO™	Cat#21875034
DMEM high glucose/F12 medium	UCSF CCF facility	N/A

(*Continued on next page*)

Continued

REAGENT or RESOURCE	SOURCE	IDENTIFIER
Fetal bovine serum (FBS)	Sigma	Cat# F4135
Penicillin-Streptomycin	GIBCO™	Cat#10378016
Lipofectamine-2000	Thermo Fisher Scientific	Cat#11668019
DNase I	Sigma-Aldrich	Cat#11284932001
ACK lysis buffer	Thermo fisher	Cat#A1049201
Collagen D	Worthington Biochemical	Cat#LS004210
TPCK trypsin	Worthington Biochemical	Cat# LS003741
Dako Target Retrieval Solution, Ph9.0	DAKO Agilent	Cat# S236784-2
Zeocin™ Selection Reagent	GIBCO™	Cat# R25001
Gentamicin	Sigma	Cat# G1397
Critical commercial assays		
KAPA Stranded RNA-Seq Kit (24rxn)	Roche	Cat#KK8400
KAPA Library Quantification Kit	Roche	Cat# KK4844
KAPA SYBR FAST Bio-Rad	Roche	Cat#KK4608
AMPure XP magnetic beads	Beckman Coulter	Cat#A63880
T7 RiboMAX™ Express Large Scale RNA Production System	Promega	Cat# P1320
Deposited data		
Raw tissue RNaseq	This paper	SRA, BioProjects #PRJNA781226
Experimental models: Cell lines		
HeLaS3	ATCC	CCL-2.2
Calu-3	ATCC	HTB-55
HeLaH1	ATCC	CRL-1958
RD	ATCC	CCL-136
Vero-E6	ATCC	1586
MDCK	ATCC	CCL-34
A549-Ace2	a gift form Peter Jackson lab (Stanford university).	N/A
Packaging cell lines (HelaS3/P1)	This paper	N/A
Vero-TMPRSS2	a gift form Whelan lab (Washington University)	N/A
Experimental models: Organisms/strains		
K18-hACE2 mice, (B6. Cg-Tg(K18-ACE2) 2Prlmn/J, Hemizygous)	The Jackson laboratory https://www.jax.org/strain/034860,	stock number: 034860
C57BL6TgPVR	a gift form Dr. Satoshi Koike of Tokyo Metropolitan Institute for Neuroscience ("TOKYO")	N/A
C57BL6TgPVR IFNAR$^{-/-}$	a gift form Dr. Satoshi Koike of Tokyo Metropolitan Institute for Neuroscience ("TOKYO")	N/A
Oligonucleotides		
The primers and probe for PV1 genomes	Integrated DNA Technologies	5′-CCACATACAGACGATCCCATAC-3′, 5′-CTGCCCAGTGTGTGTAGTAAT-3′, and 5′-6-FAM-TCTGCCTGTCACTCTCTCCAG CTT-3′-BHQ1.
The primers and probe for eTIP1 genomes	Integrated DNA Technologies	5′-GACAGCGAAGCCAATCCA-3′, 5′-CCA TGTGTAGTCGTCCCATTT-3′, and 5′-HEX-ACGAAAGAG/ZEN/ TCGGTACCACCAGGC-3′-IABkFQ.
NEXTFlex RNA-Seq Barcodes	BIOO Scientific	CAT#512914

(*Continued on next page*)

Continued		
REAGENT or RESOURCE	SOURCE	IDENTIFIER
Recombinant DNA		
Polio-PV1 plasmid	This paper	N/A
Polio-eTIP1 plasmid	This paper	N/A
Software and algorithms		
R	R	https://cran.r-project.org/mirrors.html
Graphpad prism8.0	GraphPad Software	https://www.graphpad.com/scientific-software/prism/
Flowjo	Tree Star, Inc.	https://www.flowjo.com/solutions/flowjo/downloads
ImageJ/Fuji	ImageJ	https://imagej.net/software/fiji/downloads
Other		
gentleMACS – C tubes	Miltenyi Biotec	Cat# 130-093-237
gentleMACS – M tube	Miltenyi Biotec	Cat# 130-093-236
NEXTflex™ polyA beads	Bioo Scientific	Cat# 512979
Countess™ Cell Counting Chamber Slides	Thermo Fisher Scientific	Cat# C10228
Trypan Blue solution	Sigma-Aldrich	Cat# T8154-100ML
CountessTM II automated cell counter	Thermo Fisher Scientific	Cat# AMQAX1000
Illumina HighSeq 4000	Illumina, Inc.	Cat#SY-401-4001
gentleMACS dissociator	Miltenyi Biotec	Cat#130-093-235
BD FACSAria II	BD Biosciences	N/A

RESOURCE AVAILABILITY

Lead contact

Further information and requests for resources and reagents should be directed to and will be fulfilled by the lead contact, Raul Andino (raul.andino@ucsf.edu).

Materials availability

All unique/stable reagents generated in this study are available from the Lead Contact without restriction.

Data and code availability

Raw tissue RNAseq data are publicly available. Raw tissue RNaseq data have been submitted to NCBI Sequence Read Archive BioProjects #PRJNA781226.

Any additional information required to reanalyze the data reported in this paper is available from the lead contact Raul Andino (raul.andino@ucsf.edu).

EXPERIMENTAL MODEL AND SUBJECT DETAILS

Cells lines

Cells used for this study include HeLaS3 cells, Calu-3 cells, A549-Ace2, HelaS3/P1 cells, HeLa H1 cells, RD cells, Vero-E6 cells, MDCK cells, and Vero-TMPRSS2 cells.

HeLaS3 cells (ATCC, CCL-2.2), Calu-3 cells (ATCC, HTB-55), A549-Ace2 cells were cultured in DMEM high glucose/F12 medium supplemented with 10% fetal bovine serum (Sigma) and 1x penicillin/streptomycin/glutamine (100xPSG, GIBCO). Packaging cell line: HelaS3 cells stable overexpression poliovirus P1 gene (HelaS3/P1) were cultured in DMEM high glucose/F12 medium supplemented with 10% fetal bovine serum (Sigma) and 1x penicillin/streptomycin/glutamine (100xPSG, GIBCO) plus 0.015% Zeocin (Invitrogen). HeLa H1(ATCC, CRL-1958) cells or RD cells (ATCC, CCL-136) were cultured in DMEM /H21 medium supplemented with 10% fetal bovine serum (Sigma) and 1x penicillin/streptomycin/glutamine (100xPSG, GIBCO). African green monkey kidney Vero-E6 cell line (ATCC#1586) was maintained in Minimum Essential Medium (MEM, GIBCO) supplemented with 10% fetal bovine serum (FBS, GIBCO), 1% Penicillin-Streptomycin-Glutamine (GIBCO) at 37°C in a humidified 5% CO2 incubator. A549-ACE2 cells are stable expression under-CMV promoter, a gift form Peter Jackson lab (Stanford university). MDCK(ATCC, CCL-34) was maintained in Minimum Essential Medium (MEM, GIBCO) supplemented with 8.5% fetal bovine serum (FBS, GIBCO), 1% Penicillin-Streptomycin-Glutamine (GIBCO). Vero-TMPRSS2

cells, a gift form Whelan lab (Washington University), were maintained in DMEM high glucose/F12 medium supplemented with 1x sodium pyruvate, 1x penicillin-streptomycin-glutamine and 10% FBS.

Plasmids

Plasmids with cDNA were used in this study. The Mahoney strain of poliovirus Type 1(PV1) was used as wild type PV1 in this study. Defective interference genomes (eTIP1) was used as eTIP1. (See Methods details).

Viruses

PV1, PV3, CVB3, EV-A71, EV-D68, Rhinovirus A16, and Rhinovirus 1B viruses are **Andino** lab stocks. Influenza A virus strain A/PR/8/34 (H1N1) is a gift from the Professor Christopher Byron Brooke (University of Illinois). A clinical isolates: SARS-CoV-2 (USA-WA1/2020, BEI Cat No: NR-52281), SARS-CoV-2 strain(D614G) is a gift from Sara Sunshine (UCSF). SARS-CoV-2, B1.4.27 strain is a gift from from Charles Chiu lab(UCSF), SARS-CoV-2, B1.1.7, SARS-CoV-2, B.1.617.2 are **Andino** lab stocks (See Method details).

Mice strains

Mice strains used in this study include K18-hACE2 mice, C57BL6TgPVR and IFNAR$^{-/-}$ mice.

K18-hACE2 mice (Winkler et al., 2020) (The Jackson laboratory, https://www.jax.org/strain/034860, stock number: 034860, B6.Cg-Tg(K18-ACE2)2Prlmn/J, Hemizygous).

C57BL6TgPVR and IFNAR$^{-/-}$ mice were kindly provided by Professor Julie Pfeiffer of the University of Texas Southwestern Medical Center, and originally were generated by Dr. Satoshi Koike of Tokyo Metropolitan Institute for Neuroscience (“TOKYO”) (Ida-Hosonuma et al., 2005). We followed protocols approved by the UCSF Institutional Animal Care and Use Committee (IACUC) for the mouse studies.

METHOD DETAILS

In vitro transcription (IVT) RNAs, transfection and eTIP1 production

To generate viruses and eTIP1 particle, T7 polymerase was used to generate in *vitro* transcribed (IVT) viral RNA derived from corresponding linearized prib (+) XpA Mahoney or eTIP1 plasmid by Apa1. The resulting 10 μg IVT RNA of PV1 were electroporated into 8x10^6 HeLaS3 cells. And IVT RNAs of eTIP1 were electroporated into 8x10^6 packing cells line. The detail methods as below. Monolayer of HeLaS3 or Packaging cells was trypsinized and washed three times in D-PBS. Cells were resuspended in D-PBS and the number of cells were counted on a hemo-cytometer, adjusting the concentration to 10^7 cells per ml. 800 μL of cells and 10 μg IVT RNAs were transfer into a chilled 4-mm electroporation cuvette and incubated 20 min on ice. Cells were electroporated with IVT RNAs (voltage = 200 V, capacitance = 1000 μF) using Gene Pulser I (Bio-Rad) and recovered in 8 mL pre-warmed medium (Burrill et al., 2013a, 2013b). Viruses and eTIP1 were harvested at around 24 h (or total CPE) to generate P0 virus or eTIP1 stocks. P0 virus stock were amplified once in cultured HeLaS3 in 2% serum media at M.O.I ~0.2 to generate a passage 1 (P1) stocks. P0 eTIP1 stocks were amplified once in cultured packaging cell line in 2% serum media at M.O.I ~0.2 to generate a passage 1 (P1) stocks.

Titration of virus and eTIP1 samples

Monolayers of HeLaS3 cells in 6-well plates were infected with 250 μL of serially diluted virus samples then incubated at 37°C for about 30 min, then 1% agarose overlay were added on the top. For titer eTIP, HeLaS3 cells were grown in 48-wells plate. On the following day, 100ul, 10-folds serially diluted eTIP1 samples were added to each well. Then incubation for 1 h, 400ul regular medium was added into each well. At 8-9 h post-infection, GFP-positive cells were counted as the eTIP1 titers and represent IU/mL. To measure the EV-D68 infected samples, TCID50 were performed on RD cells. RD cells were seed to 96 wells plate in 2%FBS DMEM/H21 medium with 10^4 cells per well one day before performing the TCID50.

Design of primers and Taqman probes (Droplet PCR)

Primers and Taqman probes for droplet digital PCR assay were designed with PrimerQuest Tool (Integrated DNA Technologies). The primers and probe for PV1 genomes are 5′- CCACATACAGACGATCCCATAC-3′, 5′-CTGCCCAGTGTGTGTAGTAAT-3′, and 5′-6-FAM-TCTGCCTGTCACTCTCTCCAGCTT-3′-BHQ1. The primers and probe for eTIP1 genomes are 5′-GACAGCGAAGCCAATCCA-3′, 5′ CCATGTGTAGTCGTCCCATTT-3′, and 5′-HEX-ACGAAAGAG/ZEN/TCGGTACCACCAGGC-3′-IABkFQ.

Droplet digital PCR assay. 2 μL of serially diluted cDNA samples was mixed with 10 μL of 2x ddPCR super-mix for probes (Bio-Rad), 1 μL of 20x PV1 or eTIP1 primers/probe, 1 μL of 20x eTIP1 primers/probe, and 6 μL of nuclease-free water. 20 μL reaction mix of each sample was dispensed into the droplet generator cartridge, followed by droplet production with QX100 droplet generator (Bio-Rad). Then PCR was performed on a thermal cycler using the following parameters: 1 cycle of 10 min at 95°C. 60°C of 1 min for 40x cycles. Then the PCR product were read and calculated by QX100 droplet reader.

Virus growth curve of PV1 or other wildtype viruses and co-infected replication kinetics in cell culture models

2.5 × 10^5 HelaS3 cells were seeded in 24-well plates. On the following day, cells were washed twice with PBS and were infected with virus in 200 μl, 2% serum media at M.O.I = 0.1 with virus alone or co-infected with mixed virus +eTIP1 (at ratio: 1:10, 1:20, 1:50, 1:100)

or with eTIP1 alone at MOI is 5 (three replicate wells were used for each virus at each time point). Following an h incubation at 37°C, each well was washed twice with PBS, and cells were covered with fresh complete media. At each indicated time point, the corresponding plate was frozen at −80°C. Following three freeze-thaw cycles of the plates, standard plaque assays were performed on monolayer HeLaS3 cells grown in a 6-wells plate (~10^6 HeLaS3 cells per well). Or TCID50 for EV-D68 on RD cells.

Purification of the eTIP1 particles

Packaging cell lines (HelaS3/P1) generating eTIP1 (500 ml) was harvested with 0.5% NP-40, and the sample was stored at −80°C. For virus purification, the sample was subjected to three freeze-thaw cycles. For virus precipitation, PEG 8000 was added to a final concentration of 10% and stored overnight at 4°C. The precipitated sample was pelleted by spinning at 3,500 g for 1 h. The pellet was suspended in 10 mL EB-buffer (50mM Tris pH 8.0, 300 mM NaCl, 5 mM MgCl2, 0.5% NP-40) and centrifuged at 3,500 g for 30 min at 4°C to remove cell debris and insoluble materials. The soluble fraction containing eTIP1 in the supernatant was overlayed on a 2 mL 30% sucrose cushion in EB-buffer at 105,000 g for 3 h at 4°C. The pellet was suspended in EB-buffer and centrifuged at 12,000 g for 30 min at 4°C to remove insoluble material. The soluble fraction containing eTIP1 was then laid on the top of a 15%–45% sucrose gradient in EB-buffer and centrifuged at 105,000 g for 3 h at 4°C. Fractions of 1 mL size from top of the gradient was collected containing eTIP1. Two fractions from top were pooled together, and sucrose in the sample was removed using a spin desalting column (Zebra; Pierce) and buffer exchanged with PBS. eTIP1 in PBS were then concentrated using Amicon ultra device with 100 kDa MWCO. Purity and integrity of the eTIP1 were tested by SDS-PAGE, silver staining. Negative stain and electro-microscopy were used on the particle. Franction#5-6 is combined, titered and used to inoculate into mice.

Infection of susceptible mice

We followed protocols approved by the UCSF Institutional Animal Care and Use Committee (IACUC) for the mouse studies. In these experiments, 5 to 6-weeks-old C57BL6TgPVR or 6 to 8-weeks-old C57BL6 TgPVR interferon α/β receptor knockout ($IFNAR^{-/-}$) both male and female mice were used and infected under anesthesia. C57BL6TgPVR and $IFNAR^{-/-}$ were kindly provided by Professor Julie Pfeiffer of the University of Texas Southwestern Medical Center, and originally were generated by Dr. Satoshi Koike of Tokyo Metropolitan Institute for Neuroscience ("TOKYO") (Ida-Hosonuma et al., 2005).

For mice survival studies, mice were injected by intraperitoneal injection (IP, 100 μL per mouse), by intranasal injection (IN, 20-50ul per mouse) with serial dilutions of each virus, respectively (10 mice per group) (Nagata et al., 2004). If UV- treatment was involved, then the eTIP1 were UV-treatment for 2 h. For the influenza H1N1(PR8 strain) experiment, the mouse will weight daily. Mice were monitored twice daily for the onset of paralysis and were euthanized when death was imminent.

For protection study on poliovirus, we injected C57BL6 TgPVR mice with viral supernatant 10^7 pfu of PV1 alone or with eTIP1 ratio at 1:1, 1:10 per mouse by IP route or 1:20 by I.N. route (PV1 is $3x10^5$ pfu per mouse), For tissue distribution studies, we injected C57BL6 TgPVR mice (3 to 5 mice per group) with $3x10^5$ pfu of PV1 virus per mouse by intranasal(IN) route, Half of the organs were collected from infected mice and homogenized in 1 mL serum-free media. Viral supernatants were collected from the tissue homogenates, following three freeze-thaw cycles, and centrifuged at 5,000 g for 10 min in a bench top centrifuge at 4°C. Regular plaque assays were performed on HeLaS3 cells to titer viral supernatants from tissues. For protection study on CVB3 virus, we injected Tg21 mice with viral supernatant 10^5 pfu of PV1 alone or with eTIP1 ratio at 1:100, 1:10 per mouse by IP route 24 h or 48 h post-infection, animals were weighted and checked daily.

For the pre-treat experiments, we inoculated C57BL6 TgPVR mice with $6x10^6$ IU eTIP1 particles in PBS by intranasally. 24 h and 48 h inoculation, $3x10^5$ pfu PV1 or 10^5 pfu influenza(A/PR8) virus was inoculated into Tg21 mice. For the therapeutics experiments on poliovirus, we inoculated C57BL6 TgPVR mice, $3x10^5$ pfu PV1 by intranasally at day 0, then inoculated with $6x10^6$ IU eTIP1 in PBS by intranasally daily from day1 to day5. For the therapeutics experiments on flu, 10^5 pfu influenza(A/PR8) by intranasally at day 0, then inoculated with 30ug eTIP1 RNA at 24- or 48 h post-infection.

For tissue distribution studies, The $IFNAR^{-/-}$ mice were inoculated by I.M. route with 200 pfu PV1 alone or with eTIP (PV1: eTIP1 at ratio = 1:5000) per mouse (3 mice per group). Mice were euthanized with CO2, muscle, spleen, spinal cord were collected and at 1, 3, 6 days post infection. The tissues were homogenized in 1 mL Trizol reagents (Ambion). Total RNAs were extracted and treated with Dnase1(NEB). RT-qPCR were formed as droplet qPCR section.

SARS-CoV-2 virus propagation and infection

SARS-CoV-2 cell culture and animals works were performed in the Biosafety level 3(BSL-3), under the guidance and protocols approved by UCSF Biosafety and Animal research committees.

African green monkey kidney Vero-E6 cell line (ATCC#1586) and Calu-3 cells (ATCC® HTB-55) was obtained from American Type Culture Collection (ATCC#1586) and maintained in Minimum Essential Medium (MEM, GIBCO Invitrogen) supplemented with 10% fetal bovine serum (FBS, GIBCO Invitrogen), 1% Penicillin-Streptomycin-Glutamine (GIBCO Invitrogen) at 37°C in a humidified 5% CO2 incubator. A clinical isolate of SARS-CoV-2 (USA-WA1/2020, BEI Cat No: NR-52281 with D614G) or 2 or variants of concerns (V.O.C), was propagated in Vero E6 cells and A549-ACE2 cells. Viral titer was quantified with plaque assay. All the infections in the context of SARS-CoV-2 were performed at biosafety level-3 (BSL-3).

For prophylactic and coinfection experiments, ~70% monolayers of Calu-3 cells (1×10^5 cells/well in 24-well plates) were pretreated with eTIP1 particles with MOI = 5 for 5 h (pretreatment), then infected with SARS-CoV-2 (MOI = 0.1) for 1 h at 37 °C, the virus mixture was removed, cells were further cultured with medium. At indication time-point 16, 24, 36, 48 hpi (h post infection), supernatants were collected, and viral titers of supernatant were detected with plaque assay.

For co-infection experiment, Calu-3 cells were infected with SARS-CoV-2 (MOI = 0.1) alone or co-infected with eTIP1 particles at different ratios (1:1, 1:10, 1:50) for 1 h at 37 °C. the virus mixture was removed, cells were further cultured with medium. At indicated time-points, 24, 36, 48 hpi (h post infection), supernatants were collected, and viral titers of supernatant were measured with plaque assay on Vero-E6 cells.

Plaque assay for SARS-CoV-2

For SARS-CoV-2 plaque assays, 80% Confluent monolayers of Vero E6 cells for (D614G) or Vero-TMPRSS2 (for V.O.C. B1.1.7 or B1.4.27), grown in 6-well plates were incubated with the serial dilutions of virus samples (250 μl/well) at 37 °C for 1 h. Next, the cells were overlayed with 1% agarose (Invitrogen) prepared with MEM supplemented containing 2% fetal bovine serum. Three days later, cells were fixed with 4% formaldehyde for 2 h, the overlay was discarded, and samples were stained with crystal violet dye.

Mouse experiments for SARS-CoV-2

K18-hACE2 mice (Winkler et al., 2021) (The Jackson laboratory, https://www.jax.org/strain/034860, stock number: 034860, B6. Cg-Tg(K18-ACE2)2Prlmn/J, Hemizygous). TheK18-hACE2 mice were inbred and housed in UCSF animal facility. All the experiments we performed, the mice were under anesthesia and at the BSL3 level. For prophylactic protection experiments, 30 μg eTIP1 RNA with lipofectmaine-2000 were inoculated into mice intranasally, 18-20 h later, K18-hACE2 mice were anesthetized with isofluorance and inoculated with $6x10^4$ pfu of SARS-COV-2 intranasally, mice were monitored daily, and weight were measured at indicated time-points. For therapeutic experiments for eTIP1, K18-hACE2 mice were anesthetized and infected with SARS-CoV-2 or variants of concerns (V.O.C), then the eTIP1 RNA were delivered with lipofectmaine-2000 at 24 hour, 48 hour, 24 and 48 h. For tissue distribution, mouse will be sacrificed at indication time-points, the tissues will be collected and homogenized with 1ml 2% FBS MEM medium with gentleMACS - C tubes (Miltenyi Biotec Catlog# 130-093-237), plaque assays were performed for titration of the virus. For RNA extraction, the 100mg tissues were homogenized in 1ml trizol reagents (Ambion) with gentleMACS - M tube (Miltenyi Biotec, Catlog# 130-093-236), RNA were treated with DNase1, 1mg total RNA were used to make cDNA by Iscript (Bio-Rad). DNase1 treated total RNA, then poly A beads purification (Bioo Scientific), then the RNASeq libraries will be prepared with the KAPA biosystem (KAPA Stranded RNA-Seq Library Preparation Kit).

Examining production of neutralizing antibodies

SBackspace6 to 8 weeks old C57BL6 TgPVR mice were inoculated with 30 μg eTIP1 RNA with lipofectmaine-2000 or empty lipofectmaine-2000 were inoculated into mice intranasally, 20-24 h later, mice were anesthetized with isofluorance and inoculated with 10^5, 10^4, 10^3 pfu of SARS-COV-2 (B1.1.7 strain) intranasally, for detect neutralizing antibody, blood were collected at 21days post-infection, sera were collected, then the neutralization antibody titer were determined by PRINT assay on Vero-TMPRSS2 cells.

For viral loads experiments on B.1.1.7 (Figure 6), C57B/6j Mice were sacrificed, and lungs were collected at 3 days post-infection, weighted and homogenized with 1ml 2% FBS MEM medium with gentleMACS - C tubes (Miltenyi Biotec Catlog# 130-093-237), plaque assays were performed on Vero-TMPRSS2 cells for titration of the virus.

Sera were two folds series diluted start at 20-folds dilution in 2% FBS MEM, then incubate with equal volume with SARS-CoV-2 virus (2000PFU per ml) at 37C for 2 hours, then plaque assay were performed on Vero-TMPRSS2 cells.

Hematoxylin Eosin (H&E), Immunofluorescence (IF) staining on tissue section and imaging

For pathology and immuno-fluorescence, mice tissues were collected and fixed in the 4% PFA, then the tissues were embedding with paraffin and wax, then processed and the tissue samples will cut at 5 μM, and H&E staining were performed at the Gladstone Histology and light core.

Deparaffinization, rehydration, and HIER were performed on an a ST4020 small linear stainer (Leica). For deparaffinization, slides were baked at 70 °C for 1–1.5 h, followed by rehydration in descending concentrations of ethanol (100% twice, 95% twice, 80%, 70%, ddH2O twice; each step for 30 s). Washes were performed using a Leica ST4020 Linear Stainer (Leica Biosystems, Wetzlar, Germany) programmed to three dips per wash for 30 s each. H& E staining were performed. For I.F., HIER was performed in a Lab VisionTM PT module (Thermo Fisher) using Dako Target Retrieval Solution, pH 9 (S236784-2, DAKO Agilent) at 97 °C for 10 min and cooled down to 65 °C. After further cooling to room temperature for 30 min, slides were washed for 10 min three times in Tris-Buffered Saline (TBS), containing 0.1% Tween 20 (Cell Marque; TBST). Sections were then blocked in 5% normal donkey serum in TBST at room temperature for 1 h, followed by incubation with primary antibodies in the blocking solution. After one overnight incubation of primary antibodies in 4 °C, sections were washed three times with TBST and stained with the appropriate secondary antibodies in PBS with 3% bovine serum albumin, 0.4% saponin, and 0.02% sodium azide at room temperature for 1 h. Following this, sections were washed three times with TBST and mounted with ProLong Gold Antifade mounting medium with DAPI (Invitrogen). The primary antibodies and final titrations used were mouse anti-acetylated α Tubulin (ACTUB) (1:300; Santa Cruz sc-23950), rabbit anti-SARS-CoV-2 nucleocapsid(N) (1:1000; GeneTex GTX135361), and mouse anti-SARS-CoV-2 spike(S)

(1:600; GeneTex GTX632604). Secondary antibodies include highly cross-adsorbed donkey anti-rabbit Alexa Fluor 647 1:500 (Thermo A32795) and highly cross-adsorbed donkey anti-mouse Alexa Fluor 555 1:500 (Thermo A32773). The Immunofluorescence (IF) for poliovirus eTIP1 inoculated mice head and lung sections, antibody against-poliovirus antibody 3B(Vpg) (1:200).

Fluorescence-immunolabeled images were acquired using a Zeiss AxioImager Z1 microscope or Keyence BZ-X710 fluorescent microscope. Post-imaging processing was performed using FIJI / ImageJ. The intensity of nucleocapsid(N) and spike (SP) were qualified by mean intensity of the at least ten areas at same places in each tissue section. Figures were organized using Adobe Illustrator.

Mouse lung histological analysis

Paraffin-embedded lung tissue blocks for mouse lungs were cut into 5 μm sections. Sections were stained with hematoxylin and eosin (H&E) and analyzed. Digital light microscopic scans of whole lung processed *in toto* were examined by an experienced veterinary pathologist. Hematoxylin Eosin(H&E) stained sections of lung from K18 hACE2 mice were examined by implementing a semi-quantitative, 5-point grading scheme (0 - within normal limits, 1 - mild, 2 - moderate, 3 - marked, 4 - severe). that considers four different histopathological parameters: 1) perivascular inflammation 2) bronchial or bronchiolar epithelial degeneration or necrosis 3) bronchial or bronchiolar inflammation and 4) alveolar inflammation. These changes were absent (grade 0) in lungs from vehicle and eTIP1 treated uninfected mice from groups that were utilized for this assessment (Meyerholz and Beck, 2020; White et al., 2021).

Flowcytometry analysis of the immune cells profiling from lung

For the prophylactic experiments for poliovirus challenging, we inoculated 6 weeks old Tg21 PVR mice with or without 30ug eTIP1 RNA with lipofectamine 2000 by intranasally. 24 h inoculation. Then mice were infected with SARS-CoV-2 intranasally, please refer to the SARS-CoV-2 mouse section. Then mice were euthanized with CO_2 and perfusion with PBS. The full lungs were removed, washed twice with PBS and RPMI-1640(GIBCO). Then were cut the whole lungs as small pieces put with 4ml digestion buffer (RPMI-1640+10mg/mL Collagen D +10mg/mL DNase1, 5% FBS) for 30mins, then the tissues were minced with 10ml syringe, and pass through with 70uM cell- strainer. Cells then spin it down and wash twice with D-PBS at 650 g at 4°C for 5mins. The red cells were lysis with ACK buffer (Thermo fisher, Cat#A1049201) for 2mins, Cells then spin it down and wash twice with D-PBS at 650 g at 4°C for 5mins. Collagen D (Worthington Biochemical, Cat# LS004210), DNase1(Sigma-Aldrich, Cat# 11284932001).

Cells were stained with trypan blue and counted. 10^6 Cells will used for full antibodies panel staining. 10^5 cells were used for live/dead staining for 15mins (eFluor 506 Fix Viability, eBioscience, Cat#65-0866-14), single antibody or unstaining cells or all antibodies. Mouse Fc block (BD PharMingen, Cat#553141) were diluted in D-PBS. Antibodies was diluted in 1:100 in BD brilliant stain buffer (BD Biosciences, Cat#563794). After all steps staining were completed, cells were fixed with 2% PFA for 30mins at 4°C, then washed with D-PBS for two times.

Samples were resuspended in 300ul FACS buffer (D-PBS +0.2% BSA +2mMEDTA). Samples were run in the BD Aries 3 and analyzed with Flowjo software.

Antibody panels (key resources table) and gating method are described in detail in Figure S2.

mRNaseq libraries preparation and analysis

Mice tissues were collected and homogenized in 1 mL Trizol reagents (Ambion). Total RNAs were extracted, 1mg treated with Dnase1(NEB). Then the mRNAs were purified by polyA beads, mRNaseq libraries were prepared by following the instruction with KAPA Biosciences. Then mRNaseq libraries were pooled and sequenced by Illumina HiSeq 4000 with single read in the UCSF core facility (Center for Advanced Technology, https://uccore.org/ucsf-center-for-advanced-technology/).

Differential gene and transcript expression analysis of mRNA-seq experiments with TopHat-Cufflinks-Cuffdiff pipeline (Trapnell et al., 2012). The Figures were plot by R, ggplot2 package. Annotation of type I ISGs was based on Liu et al. (PMID 22371602) for IFNα and Gene Ontology (GO) Biological Process "Response to interferon-beta" for IFNβ. For direct comparisons between eTIP1 particles and LNPs, transcripts were filtered for statistical significance in both datasets. Fisher enrichment analyses was performed in Perseus version 1.6.7.0, using GO annotations and the above type I ISG list. Analyses were performed separately for statistically significant transcripts that are induced (log2(FC)>0) or depleted (log2(FC)<0), and the results were filtered for intersection > 9 and enrichment > 5.

QUANTIFICATION AND STATISTICAL ANALYSIS

Data were presented as mean ± SD. Statistical analysis was performed using GraphPad Prism (GraphPad Software). Statistical significance was calculated using a two-tailed Student's t test and p value < 0.05 was considered significant. Significance is noted with asterisks as described in the figure legends. Animal experiments were not blinded or randomized, and no animals or samples were removed as outliers from the analysis. The 50% Lethal dose (LD50) and Survival curves were compared with Log-rank (Mantel-Cox) test methods performed using GraphPad Prism (GraphPad Software). p value < 0.05 was considered significant.

Supplemental figures

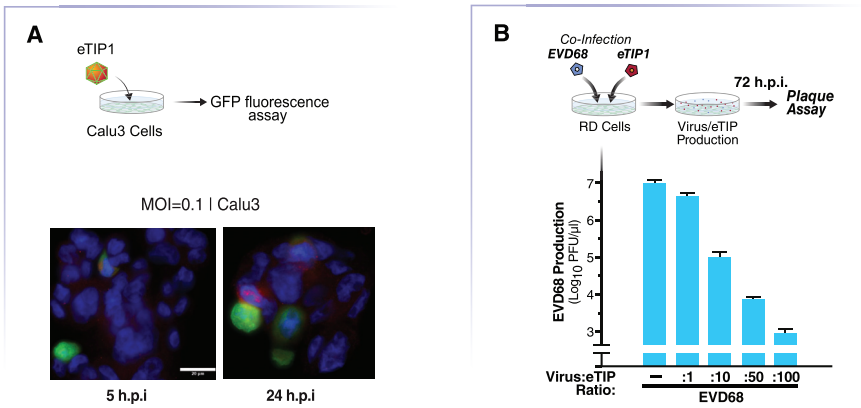

Figure S1. Replication of eTIP1 and doses-dependent effect on EV-D68 replication, related to Figure 1

(A) Immunofluorescence(IF) for eTIP1 particles on infected lung cell type, Calu-3 cells at moi = 0.1. At 5 and 24 h post-infection, cells were fixed with 4% PFA and the IF were performed with polio-3A antibody (red color) (STAR Methods).

(B) eTIP1 was to infect RD cells at different multiplicity of infection (moi) ranging from 10 to 0.1, and coinfected with EV-D68 eTIP1 (moi = 0.1). eTIP1 inhibits replication on EV-D68, implicated in outbreaks of severe respiratory illness in the US in a dose-dependent manner.

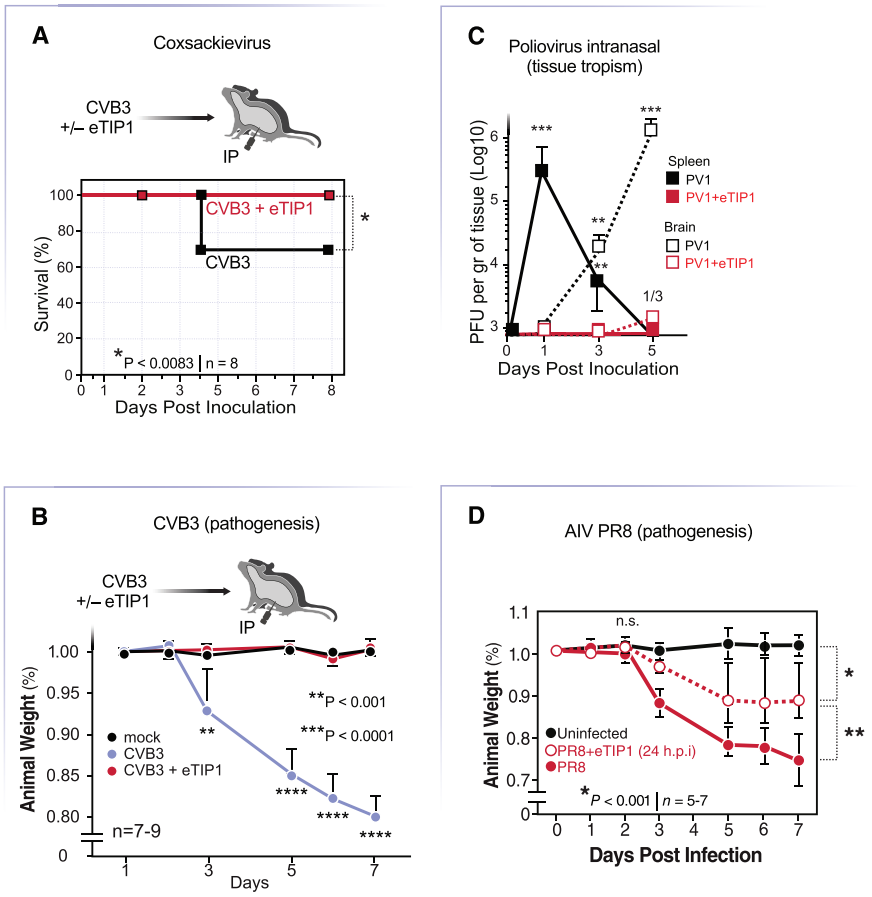

Figure S2. eTIP1 protects respiratory tract and enterovirus infection and protect from disease cause by coxsackievirus B3, poliovirus and influenza virus (AIV), related to Figure 2.

(A) Intraperitoneal inoculation in immune-competent C57BL6 TgPVR mice with 10^5 P.F.U. coxsackievirus B3 (CVB3) or co-infected eTIP1 at a ratio of 1:100(n = 7-9). Survival curve. Black line represents CVB3 alone. Red line are mice infected with a mix of CVB3 + eTIP1 group. The statistical analysis of survival curves was carried out by log-rank (Mantel-Cox) test. Significance is noted with asterisks; ns, not significant.

(B) Weight lost, experiment was carried out as in Fig.S2A. blue line represents CVB3 alone, red line are mice infected with a mix of CVB3 + eTIP1 group, black line represents mock(un-infected) control.

(C) Virus loads in spleen and brain tissues of PV1-infected (black) or PV1 + eTIP1 co-infected intranasally (IN) at a ratio of 1:20. Tissues were collected at indicated times, homogenized and tittered by plaque assay. n = 3-5. Data was analyzed using unpaired Student's t tests. Significance is noted with asterisks as follow: **p < 0.001; and ***p < 0.0001. Two independent experiments.

(D) Weight lost, red solid line represents influenza virus (PR8) alone, red dotted line are mice infected with a mix of PR8 + eTIP1 group, black line represents mock(un-infected) control(n = 5-7).. Significance is noted with asterisks as follow: *p < 0.05, **p < 0.001; and ***p < 0.0001. Two independent experiments.

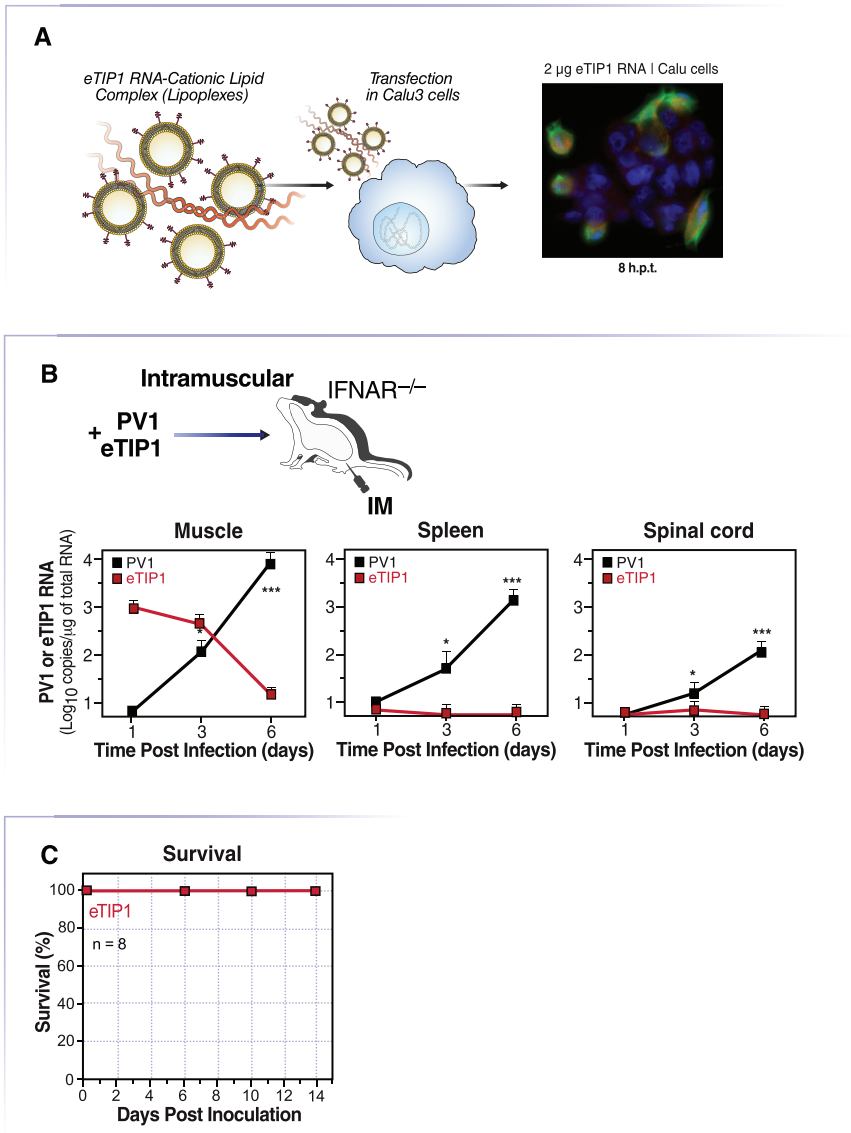

Figure S3. Delivery of eTIP1 using lipid nanoparticles (LNPs) and safety characterization of eTIP1 inoculated intramuscularly in highly susceptible mice, related to Figure 3

(A) eTIP1 RNA transfection and expression. Schematic representation of eTIP1 RNA/LNP complex. eTIP1 RNA expression in cell culture model. 2ug eTIP1 RNAs were transfected into HelaS3 cells with lipofectamine 2000, then immunofluorescence (IF) staining with the poliovirus −3A antibody at 8 h post-transfection. Poliovirus 3A protein staining (Red), eTIP1 RNA(green), the nuclear(blue).

(B) eTIP1 replication is restricted to the site of inoculation (leg muscle) even in the presence of WT polio helped virus. 6 to 8-weeks-old C57BL6 PVR interferon α/β receptor knockout ($IFNAR^{-/-}$) mice were infected with 200 P.F.U. wildtype poliovirus or co- infected with mixed PV1+ eTIP1 at ratio 1:5000 by intramuscular (I.M.) route. eTIP1 inhibits wildtype virus spread into central neuron system (CNS). However, eTIP1 replication is limited to the site of inoculation (muscle) but not spread and replicates in spleen and spinal cord. RNA genome copies for eTIP1 and PV1 by digital droplet RT-qPCR. y axis represents RNA genome copies per 1 mg total RNA. Black line with square represents as PV1 genome copies in wildtype virus alone group. Red line with square represents as PV1 genome copies in co-infection group. (n = 3). Two tails multiple-t tests. Significance is noted with asterisks as follow: *$p < 0.05$; and ***$p < 0.001$.

(C) Survival curves of mice inoculated intramuscularly with eTIP1. 6 to 8-weeks-old C57BL6 PVR interferon α/β receptor knockout ($IFNAR^{-/-}$) mice were infected with 2×10^5 P.F.U of encapsidated biological particles eTIP1.

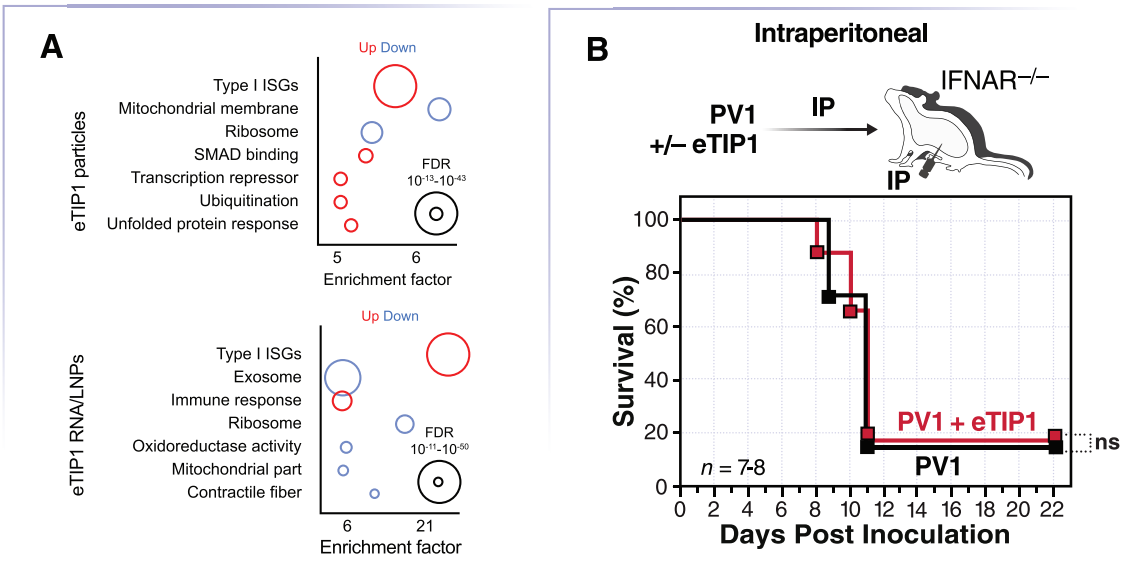

Figure S4. RNA-seq analysis of mice treated with eTIP1/LNP and the role of Type I IFN, related to Figure 3

(A) Gene Ontology (GO) annotations with manual validation were used to calculate an average fold change from mock for all host mRNA induced during eTIP1 inoculation. ANOVA p value indicated for each.

(B) eTIP1 fails to protect against poliovirus (PV1) intraperitoneally (IP) in mice lacking a type I interferon response (IFNAR$^{-/-}$). IFNAR$^{-/-}$ mice were infected with 5x10^4 pfu PV1 alone or co-infected with mixed PV1 + eTIP1 at a ratio of 1:10 by IP route. Black line represents PV1 alone. Red dash line represents co-infected mixed PV1+ eTIP1 group (n = 7-8). Data presented was collected from two independent experiments. The comparison of survival curves was performed by log-rank (Mantel-Cox) test. ns, not significant.

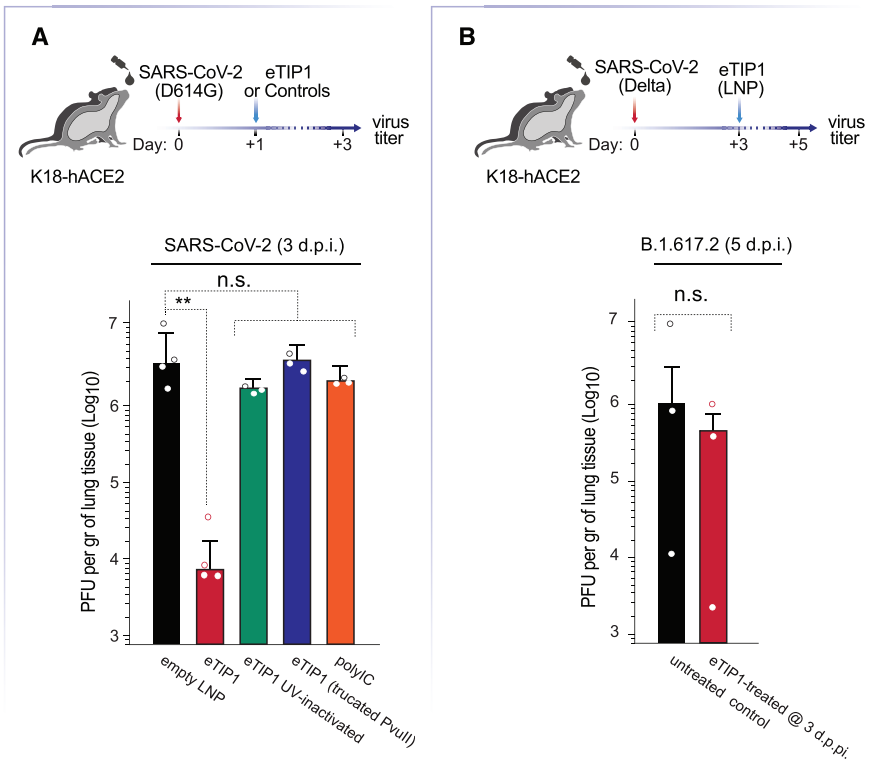

Figure S5. Only replication-competent eTIP1 protects against SARS-CoV-2, delivery of none-replicative RNA in LNP complex are not effective, related to Figures 4 and 5

(A) eTIP1 RNA/LNP and controls, e.g., UV-inactivated eTIP1 RNA, replication incompetent eTIP1 with a large deletion (~2kbps) of the most-3′ region of the eTIP1 genome, or poly IC, were inoculated into K18-hACE2 mice by the intranasal route, and at 24 h mice were infected with 10^4 P.F.U. SARS-CoV-2 D614G, B by IN route (n = 4-5). Virus titers in lugs were determined by plaque assays 3 days after infection.

(B) K18-hACE2 mice were infected by the intranasal route with 10^4 P.F.U. SARS-CoV-2 Delta variant by IN route (n = 4-5). Mice were inoculated with eTIP1 RNA/LNP (30 μg) or mock (empty LNPs) 72 h post-infection. Virus titers in lungs at 5 days post infection were determined by plaque assays. Direct animal observation suggested that eTIP1 inoculation during ongoing infection did not enhance signs of disease stress or augmented lethality of SARS-CoV-2.

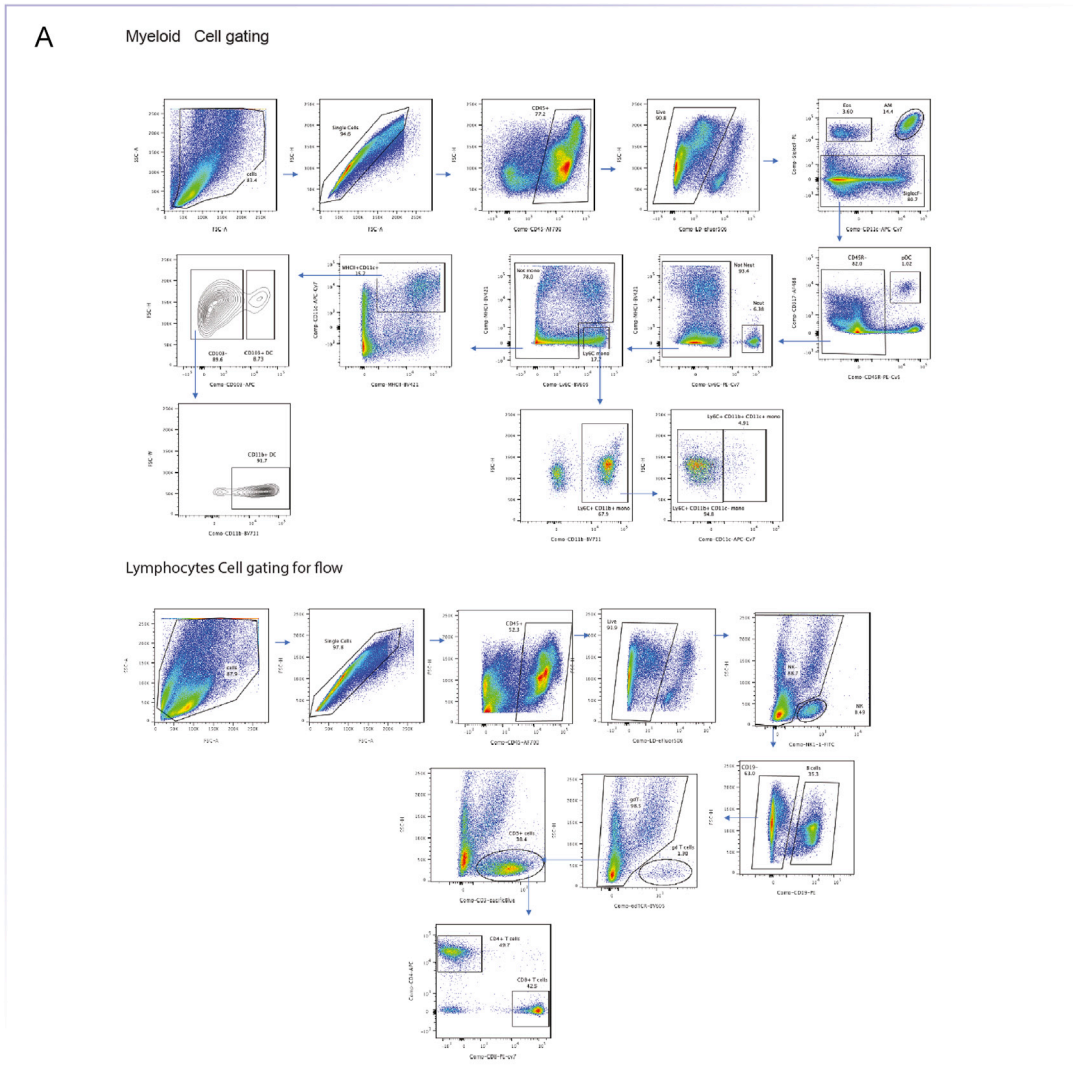

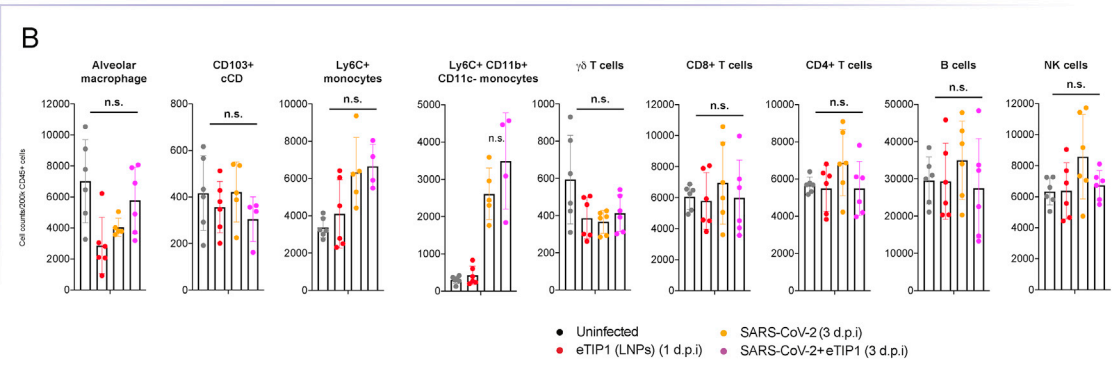

Figure S6. Gating of the flowcytometry to identify subset immune cells from the lung of eTIP1 inoculated mice, related to Figure 5

(A) Mice were perfused with PBS, lungs were collected, dissociated, red cells were lysed, single cells from each lung were obtained. Cells were counted, stainned with a flow cytometry antibody panels. Cell were then fixed with 1% PFA overnight, then washed two times with DPBS. Samples resuspend in FACS buffer and analyzed FACS machine. 200K events were collected from each sample. Data were analyzed by flowjo by sequential gating. For the first antibody panel (Myeloid Cells), from single and live cells: CD45+ cells represent as immune-cells. CD45+/SiglecF+ is eosinophils (EOS). CD45+/ SiglecF+/CD11C+ is alveolar macrophage (AM CD45+/ SiglecF-/CD317+/CD45R+ is pDC. CD45+/ SiglecF-/ CD45R- / LY6G+ is neutrophils(Neut),). CD45+/ SiglecF-/ CD45R-/ LY6G-/ LY6C+/ MHC2- is LY6C+ positive monocytes (LY6C+ Mono), CD45+/ SiglecF-/ CD45R-/ LY6G-/ LY6C+/ MHC2-/CD11b+ is LY6C+ CD11b+ positive monocytes (LY6C+ CD11b+ Mono), CD45+/ SiglecF-/ CD45R-/ LY6G-/ LY6C+/ MHC2-/CD11b+ + /CD11C+is LY6C+ CD11b+ CD11C+positive monocytes (LY6C+ CD11b+ CD11C+Mono),

(legend continued on next page)

CD45+/ SiglecF-/ CD45R-/ LY6G-/ LY6C+/ MHC2-/CD11b+ + /CD11C+is LY6C+ CD11b + CD11C-positive monocytes (LY6C+ CD11b+ CD11C-Mono). CD45+/ SiglecF-/ CD45R-/ LY6G-/ LY6C+/ MHC2+ CD11 is MHC2+ CD11+ dentritic cells(DCs), CD45+/ SiglecF-/ CD45R-/ LY6G-/ LY6C+/ MHC2+ CD11/CD103+/ Cd11b+ is LY6C+/ MHC2+ CD11/CD103+/Cd11b dentritic cells(DCs).

For the 2nd antibody panel(Lymphocytes Cell gating), from single and live cells: CD45+ cells represent as immune-cells. NK1.1+ positive cells is NK cells. NK1.1-/CD19+ cells is B cells, . NK1.1- /CD19-/gd TCR+ cells is Gammadelta TCR cells, NK1.1- /CD19-/gd TCR-/CD3+/ CD4+/ is CD4+ T cells, NK1.1- /CD19-/gd TCR-/CD3+/ CD8+/ is CD8+ T cells

Then cells numbers were calculated, data represented as cell counts group. Unpaired Student's t tests. *$p < 0.05$ as significant. **$p < 0.01$, ***$p < 0.001$. ns, no significant.

(B) Immune cell profiling (flow cytometry) of lung of mice infected intranasally with eTIP1 RNA/LNPs or mock infected. Data are represented as the number of CD45+ specific immune cells per 200,000 total cells obtained from mouse lungs (n = 3-6). Data are from two independent experiments. Unpaired Student's t tests. Significance is noted with asterisks as follow: n.s., not significant.